SOME STUDY ON HEAT TRANSFER AND PRESSURE DROP CHARACTERATICS OF CuO-DISTILLED WATER BASED NANOFLUIDS

A thesis submitted

in partial fulfillment of the requirements

for the award of degree of

Masters of Engineering

in

Thermal Engineering

Submitted by

Sunil Kumar

Regd. No. 801183020

Under the guidance of

Mr. Sumeet Sharma
Associate Professor
Department of Mechanical Engg.
Thapar University
Patiala

Dr.D.Gangacharyulu
Professor
Department of Chemical Engg.
Thapar University
Patiala

DEPARTMENT OF MECHANICAL ENGINEERING
THAPAR UNIVERSITY
PATIALA

DECLARATION

I hereby declare that the work being presented in the thesis report entitled **Some Studies on heat transfer and pressure drop characteristic of CuO-distilled water based nanofluid** by me in the partial fulfillment of the requirements for the award of degree of Masters of Engineering in Thermal Engineering, Thapar University, Patiala, is an authentic record of my own work carried under the supervision of **Mr. Sumeet Sharma**, Associate Professor Mechanical Engg. Deptt., & **Dr. D. Gangacharyulu**, Professor Chemical Engg. Deptt., **Thapar University.** The matter presented in this thesis has not been submitted in any other University/ Institute for the award of Master of Technology Degree.

Sunil

(Sunil Kumar)

This is to certify that above declaration made by the student concerned is correct to the best of my knowledge & belief.

Sumeet

(Sumeet Sharma)
Associate Professor
Department of Mechanical Engg.
Thapar University
Patiala

D. Gangacharyulu 15/7/10

(D. Gangacharyulu)
Professor
Department of Chemical Engg.
Thapar University
Patiala

CERTIFICATE

This is to certify that the thesis report entitled **Some Studies on heat transfer and pressure drop characteristic of CuO-distilled water based nanofluid** being submitted by **Sunil kumar** in partial fulfillment for the requirement of degree of **Master of Technology** in **Thermal Engineering** in the **Department of Mechanical Engineering, Thapar University, Patiala** is a record of candidate's own work carried out by him under my supervision. To the best of our knowledge, the content of this thesis does not form a basis for the award of any other degree.

(Sumeet Sharma)
Associate Professor
Department of Mechanical Engg.
Thapar University
Patiala

(D. Gangacharyulu) 15/7/13.
Professor
Department of Chemical Engg.
Thapar University
Patiala

(Countersigned by)

(Ajay Batish)
Professor & Head
Department of Mechanical Engineering
Thapar University, Patiala

(S. K. Mohapatra)
Senior professor
Dean of Academics Affair
Thapar University, Patiala

ACKNOWLEDGEMENT

I would like to express my deep sense of gratitude to Mr. Sumeet Sharma, Associate Professor, Mechanical Engg. Deptt. and Dr. D. Gangacharyulu, Professor, Chemical Engg. Deptt., Thapar University, patiala for their invaluable suggestions, excellent supervision, constant encouragement, thought provoking discussions and unabashed inspiration in nurturing the work and during the preparation of manuscript throughout the research work.

My sincere thanks to Dr. Ajay Batish, Professor & Head, Mechanical Engineering Department, Thapar University, Patiala and Dr. S.K Mohapatra, Dean of Acadmic Affair, Thapar University, Patiala, for providing me with the opportunity to conduct this work and bring it out in the present form.

I offer my special regards to Mrs. Harkirat Kaur, Research Scholars, Department of Chemical Engineering, Thapar University, Patiala, for providing their immense support in performing the experimental work throughout my research work. I would also thank to Thapar University, Patiala for providing funds to my thesis work. I would also like to thanks my friends for their kind support and encouragement.

Most importantly, I would like to thanks my family members for their infinite support at each and every part of my life. I am also thankful to my special one, Anjana Panwar for her support; love and understanding that were inevitable to make this work possible. Above all, I thanks to ALMIGHTY, for all his blessings and kindness.

Sunil

(Sunil Kumar)

ABSTRACT

In this thesis work, the heat transfer and pressure drop characteristics of the distilled water and the copper oxide-distilled water based nanofluid flowing in a horizontal circular pipe under constant heat flux condition are studied. Copper oxide nanoparticles of 40nm size are dispersed in distilled water using sodium dodecyl sulphate as surfactant and sonicated the nanofluid for three hour. Both surfactant and sonication increases the stability of the nanofluid. The nanofluids are made in three different concentration i.e. 0.1 Vol. %, 0.25 Vol. % and 0.50 Vol. %. The thermal conductivity is measured by KD2 PRO, density with pycnometer, viscosity with Brookfield LVDV-III rheometer. The results show that the thermal conductivity increases with both temperature and concentration. The viscosity and density increases with concentration but decreases with temperature. The specific heat was calculated by model and it decreases with concentration. The experimental local Nusselt number of distilled water is compared with local Nusselt number obtained by the well known shah equation for laminar flow under constant heat flux condition for validation of the experimental set up. The relative error is 4.48 % for the Reynolds number 750.9. The heat transfer coefficient increases with increase in both flow rate and concentration. It increases from 14.33 % to 46.1 % when the concentration is increased from 0.1 Vol. % to 0.5 Vol. % at 20 LPH flow rate. Friction factor decreases with increase in flow rate. It decreases 66.54 % when the flow rate increases from 10 LPH to 30 LPH for 0.1 Vol. %.

TABLE OF CONTENTS

List of Figures

List of Tables

NOMENCLATURE

Symbols

V	Voltage applied (V)
I	Current (A)
U	electrophoresis mobility ($v/V/L$)
v	velocity of the particles under an electric field in (cm/s)
L	electrode distance(cm)
D_B	Brownian Diffusion coefficient
k_B	Boltzmann constant
d_p	particle diameter (m)
A_s	Average temperature surface temperature of test section (°C)
r_o	Outside radius of the test section (m)
r_i	Inside radius of the test section(m)
L	length of the test section (m)
A_c	Cross-sectional area (m^2)
x	the axial distance from the inlet of the test section (m)
P	surface perimeter (m)
Re	Reynolds number
Nu	Nusselt number
Pr	Prandtl number
Δp	Pressure drop (Pa)
D	Tube inside diameter (m)
h	Heat transfer coefficient ($W/m^2.K$)
f	Friction factor
q	Heat flux (W/m^2)
A_s	Surface area (m^2)
C	Specific heat (J/kg.k)
$\dot{m}$	Mass flow rate (kg/s)

$\overline{V}$	Average velocity (m/s)
T_i	Inlet fluid temperature (°C)
T_o	Outlet fluid temperature (°C)
T_w	Wall temperature (°C)

Greek symbols

¨	Nanoparticles volume fraction
~	Thermal diffusivity (m^2/s)
°	Density (Kg/m^3)
«	Dynamic viscosity ($N.s/m^2$)
¸	zeta potential (mV)
£	dielectric constant of the medium

Subscripts

bf	Base fluid
nf	Nanofluid
w	Wall temperature
f	Fluid
i	Inlet
o	Outlet

Chapter – 1

Introduction to Nanofluids

1.1 Introduction

Now-a-days conventional heat transfer fluids such as air, water, helium, minerals oils, ethylene glycol and freon are inadequate for ultra-high cooling require in super computers, industries, automobile, integrated-electronic devices, fuel cell, high power microwaves tubes and superconducting magnets due to limited thermal conductivity. So, the research had been going on, to find the new method for enhancing the heat transfer from past few decades. One of the methods is incorporating the very small size particles such as metallic, non-metallic and polymeric in to base fluid to enhance the heat transfer.

Increase in thermal conductivity by suspending micrometer or millimeter size particles but these techniques had many drawback. The drawbacks are poor stability of the suspension, abrasion/erosion in pipe walls and clogging of the flow channel.

1.2 Needs of nanofluids

Cooling is one of the critical problems facing by the modern industry due to the technological development such as microelectronic devices, high power engines, and ultrahigh heat-flux optical devices. Efficient cooling system is not only necessary for the normal performance of the devices but also for its long life and reliability. Air cooling is the most basic method for cooling electronic systems. It has limitation that it is not suitable for the system producing heat fluxes more than 100 W/cm^2 and devices will require liquid cooling. In the transportation industry, high power engines or hybrid vehicles required larger radiators in the cooling system. This increases frontal areas which results in additional aerodynamic drag and increases fuel consumption. Conventional coolants and oils have inherently poor heat transfer properties. So, there is need to develop advanced cooling system and high heat transfer performance fluids than those presently available [1].

1.3 Development of nanofluids

It is well known that at room temperature, metals in solid form have orders-of magnitude higher thermal conductivities than those of fluids For example, copper has high thermal conductivity at room temperature, and is about 700 times greater than that of water and about 3000 times greater than that of engine oil. Therefore, the thermal conductivities of fluids containing suspended solid metallic or non-metallic (metallic oxide) particles would be expected to be significantly higher than those of conventional heat transfer fluids. Over the last several decades, scientists and engineers have attempted to develop fluids, which offer better cooling or heating performance for a variety of thermal systems compared to conventional heat transfer fluids. The novel concept of a nanofluid was coined by Stephen U. S. Choi at the Argonne National Laboratory of USA in 1995. Nanofluids are a new class of heat transfer fluids produced by dispersing particles (size less than 100 nm) into a conventional heat transfer fluids such as water, ethylene glycol and oils [1].

1.4 Comparison of the microparticles and nanoparticles [1]

Table 1.1: Comparison between micro and nanoparticles

S. No.	**Parameters**	**Microparticles**	**Nanoparticles**
1	Stability	Settle	Stable (remain in suspension almost indefinitely)
2	Surface/volume ratio	1	1,000 times larger than that of micro-particles
3	Conductivity (at the same volume fraction)	Low	High
4	Clog in micro-channel	Yes	No
5	Erosion	Yes	No
6	Pumping power	Large	Small
7	Nanoscale phenomena	No	Yes

1.5 Nanotechnology

Nanotechnology consists of functional materials, devices, and systems and is controlling matter at the nanoscale level, and the exploitation of their novel properties and phenomena that emerge at that scale [1].

There are mainly two approaches that are used in nanotechnology:

1.5.1 Bottom-up approach: It referred as the formation of nanoparticles from constituent atoms.

1.5.2 Top-down approach: It referred as the synthesis of nanostructures from bulk.

1.6 Nanofluids and its structure

Nanofluids are the heat transfer fluids produced by incorporating the very small size particles (average size less than 100 nm) such as metallic, non-metallic and polymeric into conventional fluid. Yu and Choi [2] modified Maxwell model with the assumption that the base fluid molecules close to the solid surface of the nanoparticles form a solid-like layered structures. Hence the nanolayer works as a thermal bridge between the liquid base fluid and the solid nanoparticles, and this will enhance the effective thermal conductivity. As seen from Fig. 1, a nanofluid consists of the liquid base fluid, the solid nanoparticles and the nanolayer.

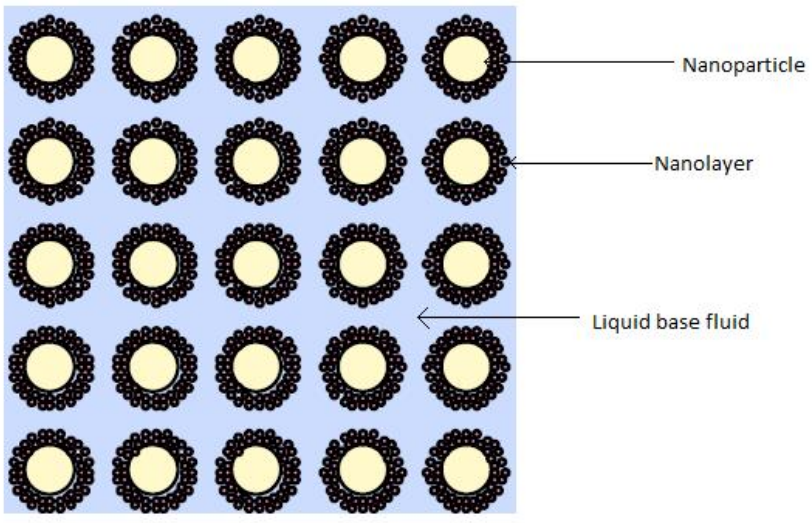

Fig. 1: Structured of Nanoparticles

1.7 Types of nanomaterials [1& 3]

Table 1.2: Types of nanomaterials

S. No.	Description	Example
1	Metals	Cu, Al, Ag, Au
2	Non-metals	Si, Al_2O_3, Graphite, Carbon nanotubes
3	Nitride ceramics	AlN, SiN
4	Carbide ceramics	SiC, TiC
5	Semiconductors	TiO_2, SiC
6	Oxide ceramics	Al_2O_3, CuO
7	Composite materials	Alloyed nanoparticles, $Al_{70}Cu_{30}$
8	Layered	Cu + C, Al + Al_2O_3

1.8 Base fluids

Base fluids are also called host fluids. They are single-phase conventional fluids having poor heat transfer properties [1 & 3].

Table 1.3: Types of base fluids

S. No.	Description	Examples
1	Metallic liquids	Sodium
2	Non-metallic liquids	Water, Ethylene glycol (EG) Engine oil (EO)

1.9 Advantages of nanofluids [4]

- Higher the specific surface area and higher the heat transfer surface between particles and fluid.
- Higher stability of the colloidal suspension due to Brownian motion of the particles.

- Lower pumping power required to achieve the equivalent heat transfer.
- Reduced particle clogging as compared to conventional colloids, hence promoting system miniaturization.
- Adjustable properties, including thermal conductivity and surface wetability, by varying particle concentrations to suit different applications

1.10 Challenges of nanofluids

i. **Long term stability of nanoparticles dispersion:** Preparation of homogeneous suspension remains a technical challenge since the nanoparticles always form aggregates due to very strong van der Waals interactions. To get stable nanofluids, physical or chemical treatment have been conducted such as an addition of surfactant, surface modification of the suspended particles or applying strong force on the clusters of the suspended particles [5]. Choi et al. [6] reported that the excess quantity of surfactant has a harmful effect on viscosity, thermal property, and chemical stability.

ii. **Increased in pumping power and pressure drop:** The pressure drop increases if nanoparticles size increase and hence power required for pumping also increases. The properties of the base fluid like density and viscosity directly influenced the pressure drop. If the viscosity and density of the fluid is increases then pressure drop and pumping power also increases.

iii. **Higher viscosity:** As the particle concentration in the suspension increases the viscosity of nanofluid also increased. So, the particle mass fraction cannot be increased unlimitedly [7].

iv. **Lower specific heat:** From the literatures, it has been found that specific heat of nanofluids is lower than base fluids. Namburu et al. [8] reported that CuO/ethylene glycol nanofluids, SiO_2/ethylene glycol nanofluids and Al_2O_3/ethylene glycol nanofluids exhibit lower specific heat compared to base fluids. An ideal coolant should possess higher value of specific heat which enables the coolant to remove more heat.

v. **High cost of nanofluids:** Higher production cost of nanofluids is among the reasons that may hinder the application of nanofluids in industry. Nanofluids can be produced by either one step or two steps methods. However both methods require advanced and sophisticated equipments. Lee and Mudawar et al. [9] and Pantzali et al. [10] stressed that high cost of nanofluids as the drawback of nanofluids applications.

References

1. S.K Das, S.U.S Choi, Y Wenhua and T Pradeep, Nanofluids: Science and Technology. John Wiley & Sons, Inc. New Jersey (2007).
2. W. Yu, S.U.S. Choi, The role of interfacial layers in the enhanced thermal conductivity of nanofluids: a renovated Maxwell model, J. Nanoparticle Res. 5 (2003) 167–171.
3. S Kakaç, A Pramuanjaroenkij, Review of convective heat transfer enhancement with nanofluids, International Journal of Heat and Mass Transfer, 52 (2009) 3187–3196.
4. SUS Choi. In: DA Singer, HP Wang, Development and application of non-Newtonian flows, New York: ASME; 231 (1995) 99–105.
5. Hwang Y, Park HS, Lee JK, Jung WH., Thermal conductivity and lubrication characteristics of nanofluids, Current Applied Physics, 651 (2006) 67–71.
6. C Choi, HS Yoo, JM Oh., Preparation and heat transfer properties of nanoparticles in transformer oil dispersions as advanced energy-efficient coolants, Current Applied Physics (2008) 710–712.
7. S Wu, D Zhu, X Li, H Li, J Lei., Thermal energy storage behavior of Al_2O_3–H_2O nanofluids, Thermochim Acta, 483 (2009) 73–80.
8. PK Namburu, DK Das, KM Tanguturi, RS Vajjha., Numerical study of turbulent flow and heat transfer characteristics of nanofluids considering variable properties, International Journal of Thermal Science, 48 (2009) 290–302.
9. J Lee, I Mudawar, Assessment of the effectiveness of nanofluids for single phase and two-phase heat transfer in micro-channels, International Journal of Heat Mass Transfer, 50 (2007) 452–63.
10. MN Pantzali, AA Mouza, SV Paras., Investigating the efficacy of nanofluids as coolants in plate heat exchangers (PHE), Chemical Engineering Science, 64 (2009) 3290–3300.

Chapter -2

Literature Review

Michael et al. [1] had presented a study of powder agglomeration and thermal conductivity in copper-based nanofluids. The synthesis of the copper powders was achieved by the use of three different surfactants (polyvinyl pyrrolidone (PVP), and cetyltrimethyl ammonium bromide (CTAB), oleic acid). Depending on the surfactant, the crystallite size and percent oxide on the powders were successfully altered. As the surfactant concentration increased the crystallite size decreased for all the powders. For CTAB and PVP, surface area increases as the crystallite size decreased. The samples synthesized in oleic acid exhibited the best oxidation protection due to the persistence of the organic layer surrounding the metal particles after cleaning. It was showed that the use of surfactants during synthesis of copper nanopowders had important consequences on the dispersion of the powders in a base fluid. The CTAB-prepared powders exhibited the best dispersion characteristics.

Dhivyaa et al. [2] synthesized cupric oxide nanoparticles by reduction of cupric acetate. 60nm wide and 260nm long needle shape particles were revealed under scanning electron micrographs (SEM). These particles were dispersed using ultra-sonication and by the use of Cetyl Trimethyl Ammonium Bromide as surfactant. Stability was ascertained by visual observation of nanofluids stored undisturbed. The zeta potential was measured to be -30 mV. The colloidal stability of CuO-water nanofluids was expected due to electrostatic and steric repulsion.

Michał et al. [3] had analyzed the stability of nanofluids obtained by suspending 30–50 nm copper (II) oxide and 10 nm γ-aluminum (III) oxide nanopowders in water with different surfactants (triammonium citrate, diammonium hydrogen citrate and sodium hexametafosfate). It was found that good stability of CuO-water nanofluid was obtained for 1% mass SHMP, and instability of CuO-water nanofluid might had been connected with the average size of particles (~400 nm) and not sufficient de-agglomeration by sonication.

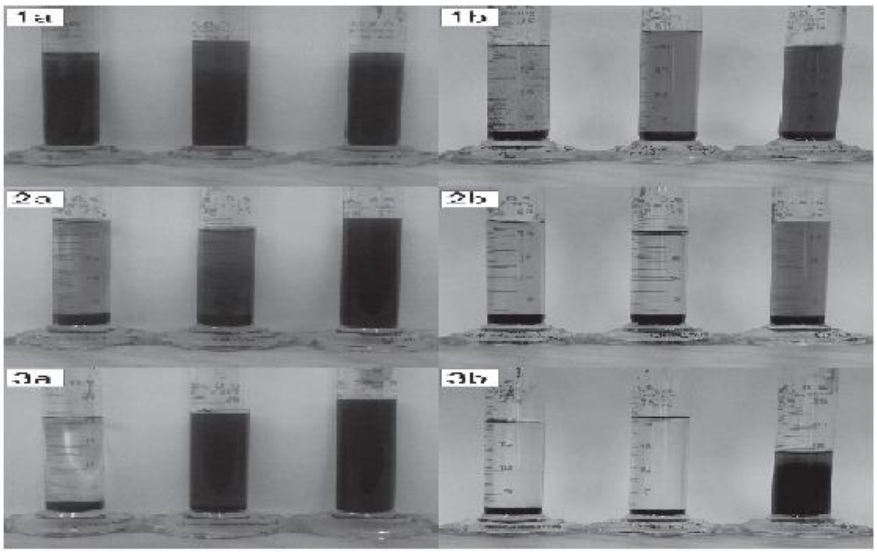

Fig. 2.1: CuO-water nanofluid after (a) 1 day, (b) 2 days stabilized by (1) triammonium citrate (from left 0.3, 0.2, 0.1% mass), (2) diammonium hydrogen citrate (from left 0.3, 0.2, 0.1% mass) and (3) SHMP (from left 3, 2, 1% mass)

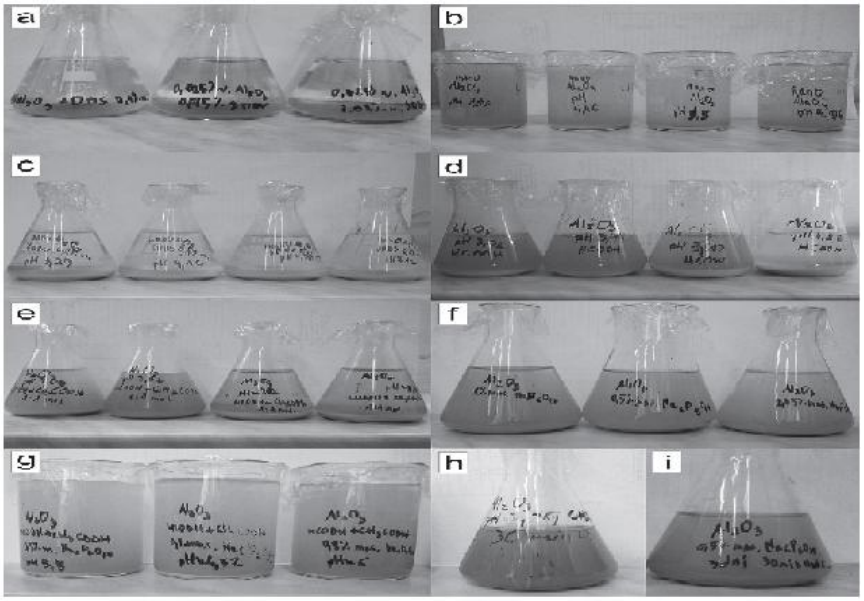

Fig. 2.2: γ-Al_2O_3-water nanofluid after a day, prepared in (a-g) 1 day (h-i) 3 day preparation procedure stabilized by (a) SDBS (from the left 0.1, 0.075, 0.03% mass), (b) acetic acid (*pH* 3.9, 4.5, 5.5, 6.8), (c) acetic acid- 0.1% mass SDBS mixture (p^H 3.4, 4.2, 4.5, 5.5), (d) formic acid (p^H 3.0, 3.4, 3.9, 4.9, (e) equi-molar acetic-formic acids mixture (p^H 3.1, 3.9, 4.5, 5.5), (f) SHMP (1, 0.5, 2.45% mass), (g) acetic-formic acids-0.5% mass SHMP mixture (p^H 3.5, 4.5, 6.0), (h) acetic acid (p^H 3.4) and (i) SHMP (0.5% mass)

It was found that poor stability of γ-Al_2O_3-water nanofluid was found for all investigated stabilizers. Instability might have been connected with the average size of particles (~400 nm) and not sufficient deagglomeration by sonication. Average particle diameter (to~250 nm) decreased if sonication time increased.

Vajjha et al. [4] had performed density measurements on three different nanofluids containing aluminum oxide, antimony-tin oxide, and zinc oxide nanoparticles in a base fluid of 60:40 ethylene glycol/water by mass. Density increased with concentration, as the nanoparticles being added was of higher density than the base fluid. The maximum deviation between experimental values and the Pak and Cho equation was about 8% for ZnO nanofluid. Deviation was increased by increasing the volume concentration. It was observed that the density decreases as the temperature of the nanofluid increases.

Sheng-Qi et al. [5] had experimentally investigated the specific heat C_p of water-based Al_2O_3 nanofluid with a differential scanning calorimeter. It was found that the specific heat $C_{p,nf}$ of nanofluid decreased with increasing nanoparticle volume fraction and their relationship was in good agreement with the prediction from the thermal equilibrium model while the other simple mixing model failed to predict the specific heat $C_{p,nf}$ of nanofluid.

Le-Ping et al. [6] had briefly defined the volumetric heat capacity and specific heat capacity measured at room temperature, were compared with two kinds of models for determination of the specific heat capacity of nanofluid. The particle size effect and particle-liquid interface effect on the specific heat capacity of nanofluid was also discussed briefly. The measurement and the prediction from the thermal equilibrium model exhibited good agreement. The other simple mixing model failed to predict the specific heat capacity of CuO nanofluid. The effect of liquid adsorption on suspended nanoparticles with increasing nanoparticles volume concentration surface would also increase the specific heat capacity of nanofluid to some extent.

Donghyun et al. [7] had used a differential scanning calorimeter instrument to measure the specific heat of the neat molten salt eutectic and after addition of nanoparticles. The specific heat of the nanofluid was enhanced by 19–24%. It was due to high specific surface energies that were

associated with the high surface area of the nanoparticles per unit volume (or per unit mass). The measurement uncertainty for the specific heat values in the experiments was estimated to be in the range of 1–5%. The experimental data contradicted earlier experimental results reported in the literature. The dispersion and stability of the nanoparticles were confirmed by using scanning electron microscopy (SEM). Transmission electron microscopy (TEM) confirmed that there was no agglomeration of the nanoparticles.

Donghyun et al. [8] had studied anomalous enhancement of specific heat capacity of high temperature nanofluids. Alkali metal chloride salt eutectics were doped with silica nanoparticles at 1% mass concentration. The specific heat capacity of the nanofluid was enhanced by 14.5%. Dispersion behavior of the nanoparticles in the eutectic was confirmed by scanning electron microscopy (SEM). Three independent competing transport mechanisms were enumerated to explain the anomalous behavior.

(1) Mode I: enhanced specific heat capacity of nanoparticle due to higher specific surface energy (compared with bulk material);

(2) Mode II: additional thermal storage mechanisms due to interfacial interactions (e.g., such as interfacial thermal resistance and capacitance) between nanoparticles and the adhering liquid molecules due to the extremely high specific surface area of the nanoparticles;

(3) Mode III: the existence of semi-solid liquid layer adhering to the nanoparticles, which was likely to have enhanced specific heat capacity due to the smaller inter-molecular spacing similar to the nanoparticle lattice structure on the surface (compared to the higher inter-molecular spacing in the bulk liquid).

Salma et al. [9] had investigated the steady-state viscosity of carbon nanotubes water-based nanofluids and the influenced of particle volume fraction and temperature ranging from 0 to 40 °C. It was showed that the nanofluids behave as shear-thinning materials for high particle content. For lower particle content, the nanofluids were quite Newtonian. It was also observed that the relative viscosity of nanofluids at high shear rate did not vary with temperature. Moreover, the evolution of relative viscosity at high shear rate was well predicted by the Marone Pierce model considering the effect of nanoparticles agglomerates.

Namburu et al. [10] had found that silicon dioxide nanofluids with ethylene glycol/water as base fluids exhibit non-Newtonian behaviour at lower temperatures. But at higher fluid temperatures it exhibited newtonian behaviour, because the curves between viscosity and shear rate was horizontal straight lines for temperatures more than -10°C. It was found that the viscosity of SiO_2 nanofluids increased as the volumetric nanoparticle concentration was increased but it decreased exponentially as the temperature increased. The specific heat of SiO_2 nanofluid decreased as the nanoparticle volume concentration increased. A new empirical correlation between the viscosity, nanoparticle volume concentration and temperature of SiO_2 nanofluid had been derived.

Murshed et al. [11] had prepared nanofluids by dispersing TiO_2 nanoparticles in deionized water. A transient hot-wire apparatus with an integrated correlation model was used to measure the thermal conductivities of these nanofluids more conveniently. Experimental results showed that with increased of particle volume fraction the thermal conductivity increased. Particle size and shape also influenced the thermal conductivity enhancement of nanofluids. The experimental results were compared with theoretical predictions by several existing models. It was found that existing models for solid–liquid mixtures, the experimental results were remarkably higher. The comparisons indicated that development of a suitable model to predict the thermal conductivity of nanofluids further research efforts was needed.

Thakleaw et al. [12] measured the thermal conductivity of TiO_2 and Al_2O_3 nanofluids experimentally. The base fluids used were water and ethylene glycol–water mixture (20/80 by mass). The measurement was done by the transient hot-wire method. The results showed that thermal conductivity of nanofluids increased more with respect to the base fluid and increased with increasing concentration and temperature. The value of thermal conductivity ratio from the experiment did not match up with that obtained from using well known models, both in terms of concentration and temperature. The newly and specifically developed correlation for predicting thermal conductivity of Al_2O_3 and TiO_2 nanofluids gave similar results to the experiment at acceptable level.

Murshed et al. [13] had conducted a combined experimental and theoretical study on the effective thermal conductivity and viscosity of nanofluids. The viscosity and thermal

conductivity of nanofluids were measured and found to be considerably higher than the values of the base fluids. Both the viscosity and thermal conductivity of nanofluids increased as the nanoparticle volume fraction increased. The thermal conductivity of nanofluids was observed to be strongly dependent on temperature. Two static mechanisms-based models were proposed to predict the enhanced thermal conductivity of nanofluids having spherical and cylindrical nanoparticles.

Laura et al. [14] had done experimental study on the stability, dynamic viscosity and thermal conductivity of water-based nanofluids containing TiO_2 nanoparticles. The measured thermal conductivity of TiO_2-water nanofluids was increased with mass concentration and with temperature. The effect of increasing conductivity was more evident at higher temperatures. All the nanofluids exhibit a Newtonian rheological behavior. The behaviour of viscosity was evaluated by means of a Rheometer in the temperature range between 283K and 343 K as a function of composition and temperature. It was found that the thermal conductivity enhancement as a function of temperature and nanoparticle concentration.

Gwon et al. [15] had adopted two different methods for producing stable CNT nanofluid because it was well-known that CNTs are hydrophobic, which was prone to aggregation and precipitation in water. Method one used a surfactant (sodium-dodecyl sulfate) for obtaining stable nanofluid. In the second method, hydrophilic functional group was attached onto the surfaces of CNTs. Nitric/sulfuric acid mixture was used to modify the surfaces of CNTs. The experimental system is shown in Fig. 3 and consisted of a magnetic chemical pump, flow-meter, test section and differential pressure transducers. The pump power was controlled by a digital inverter.

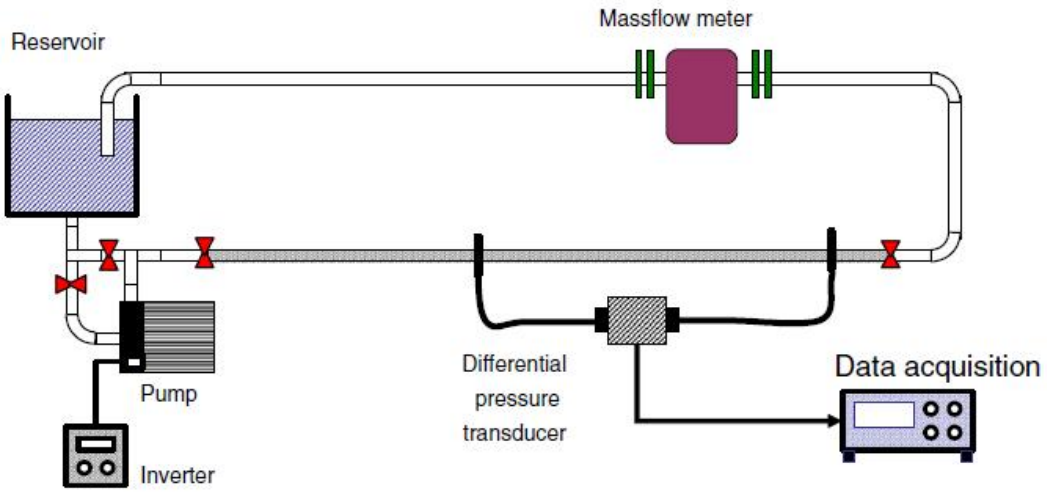

Fig. 2.3: Experimental apparatus for measuring the pressure drop in horizontal tube.

The stainless-steel tube is used in test section having tube length 4 m and tube inner diameter 10.7 mm. The first pressure tap was located at the 130-diameters downstream from the test section inlet, and the distance between two pressures taps is 2 m. Differential pressure transducers was used for measuring the pressure difference between two taps.

LI et al. [16] had built an experimental setup to examine convective heat transfer and flow characteristics of the nanofluid flowing in a tube. The experimental system is shown in Fig.2

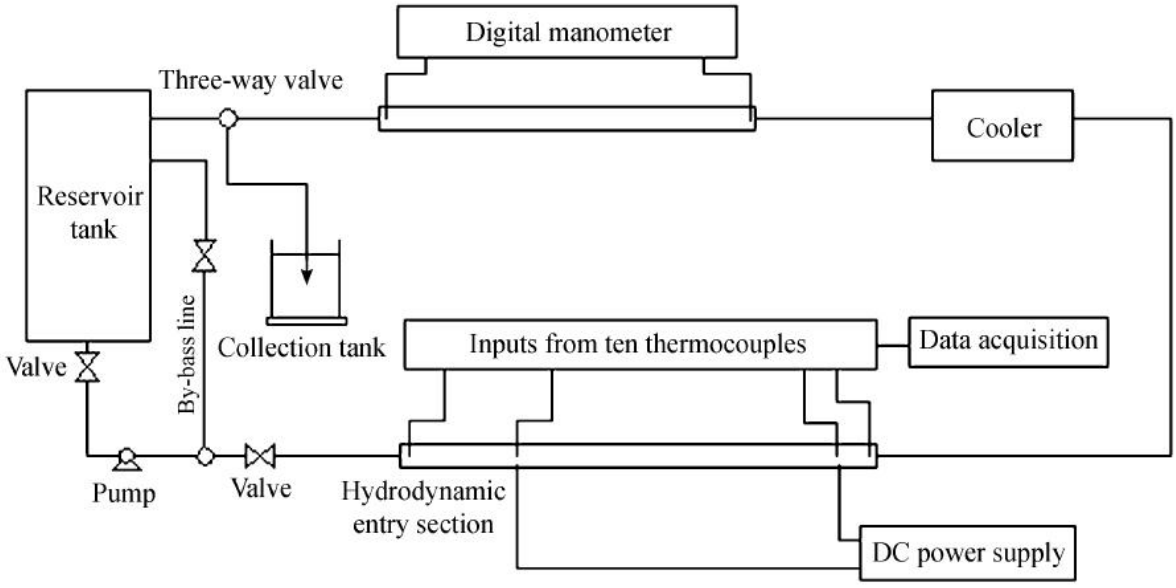

Fig. 2.4: Experimental apparatus.

It consisted of a reservoir tank, a pump, a bass line, a heat transfer test section, a cooler, a pressure drop test section and a fluid collection tank. The reservoir tank was used to deposit the nanofluid and monitor the dispersion behavior and stability of the nanofluid. The cooler was used to keep constant temperature at the inlet of the test section. The flow rate was controlled with two adjusting valves, one at the main flow loop and the other at the base line. A three-way valve enabled the flow to be diverted from the reservoir tank into the fluid collection tank in order to measure the mass flow rate of the nanofluid. The pressure drop test section was used to measure the pressure drop of nanofluid. The heat transfer test section was a straight brass tube. Ten thermocouples were mounted at different places of the heat transfer test section to measure the wall temperatures and the fluid bulk temperatures. Heat transfer test section was heated electrically by a DC power supply to obtain a constant-heat-flux boundary condition and capable of delivering a maximum power. The whole test section was thermally isolated on the outside with a layer of expanded pearl powder and a vacuum casing tube.

It was found that the suspended nanoparticles remarkably increased the convective heat transfer coefficient of the base fluid and the friction factor of the sample nanofluid with the low volume fraction of nanoparticles was almost not changed. Compared with the base fluid, for example, the convective heat transfer coefficient was increased by about 60% for the nanofluid with 2.0 vol. percent Cu nanoparticles at the same Reynolds number.

Yulong et al. [17] had done experimental study on heat transfer behaviour of aqueous suspensions of multi-walled carbon nanotubes (MWCNT nanofluids) flowing through a horizontal tube. It was found that the enhancement of convective heat transfer coefficient depends on the flow conditions (Reynolds number, Re), CNT concentration and the pH (with the effect of pH smallest). The enhancement was a function of axial distance from the inlet, increased first, reaching a maximum, and then decreased with increasing axial distance. The position at which the maximum enhancement occurred increased with CNT concentration and the Reynolds number. Given CNT concentration and pH level, there seemed to be a Reynolds number above which there was a big enhancement in the convective heat transfer coefficient occurred. Such a big increase was due to the shear thinning behavior.

Zeinali et al. [18] had done experiment with constant wall temperature and seen the convective heat transfer characteristics of Al_2O_3/water nanofluid inside a circular tube. Heat transfer coefficient increased with concentration of nanoparticles in nanofluid. The increased in heat transfer coefficient due to presence of nanoparticles was much higher than the prediction of single phase heat transfer correlation used with nanofluid properties. It was concluded that thermal conductivity increase was not the sole reason for heat transfer enhancement in nanofluids. Other factors such as dispersion and chaotic movement of nanoparticles, Brownian motion and particle migration might play role in heat transfer augmentation due to nanoparticles.

Yurong et al. [19] had measured flow and heat transfer characteristics of aqueous TiO_2 nanofluids flowing through a straight vertical pipe under both the laminar and turbulent flow conditions. It was found that:

- Addition of nanoparticles into the base liquid enhanced the thermal conduction and the enhancement increased with increasing particle concentration and decreasing particle (agglomerate) size. The shear viscosity of nanofluid decreased first with increasing shear rate (the shear thinning behaviour), and then approached a constant at a shear rate greater than 100 s^{-1}.
- Given the flow Reynolds number and particle size, the convective heat transfer coefficient increased with nanoparticles concentration in both the laminar and turbulent flow regimes and the effect of particle concentration seemed to be more considerable in the turbulent flow regimes.
- Given the particle concentration and flow Reynolds number, the convective heat transfer coefficient did not seem to be sensitive to the average particle size under the conditions of this work.
- The results also showed that the pressure drop of the nanofluid flows was very close to that of the base liquid flows for a given Reynolds number.

Anoop et al. [20] evaluated the effect of particle size on convective heat transfer in laminar developing region. Two particle sizes were used, one with average particle size off 45 nm and the other with 150 nm. It was observed that both nanofluids showed higher heat transfer characteristics than the base fluid and the nanofluid with 45 nm particles showed higher heat

transfer coefficient than that with 150 nm particles. It was also observed that in the developing region, the heat transfer coefficients showed higher enhancement than in the developed region.

Shuichi et al. [21] had performed Experimental study to investigate heat transfer performance of aqueous suspensions of nanoparticles, that is, Al_2O_3, CuO, and diamond. They found that (1) by suspending nanoparticles in base fluid the heat transfer enhancement was caused and become more prominent with increase in particle volume fraction. (2) The presence of particles produces adverse effects on viscosity and pressure loss that also increased with the particle volume fraction. The enhancement of the above properties was due to particle aggregation.

Fotukian et al. [22] had conducted an experiment to find the turbulent convective heat transfer performance and pressure drop of very dilute (less than 0.24% volume) CuO/water nanofluid flowing through a circular tube. Measurements showed that addition of small amounts of nanosized CuO particles to the base fluid increased heat transfer coefficients considerably. In average 25% increase in heat transfer coefficient was observed with 20% penalty in pressure drop. Also the ratio of convective heat transfer coefficient of nanofluid to that of pure water decreased with increasing Reynolds number. It was observed that the wall temperature of the test tube decreased considerably when the nanofluid flowed in the tube.

Chandrasekar et al. [23] had synthesized Al_2O_3 nanoparticles of 43 nm size by chemical precipitation method and prepared a nanofluid with a volume concentration of 0.1% by dispersing a specified amount of Al_2O_3 nanoparticles in distilled water. The Nusselt number was measured and was increased by 12.24% at Re = 2275 in the fully developed region for plain tube with nanofluid compared to distilled water. Two wire coil inserts made of stainless steel with pitch ratios (defined as the ratio of pitch of the coil to diameter of tube) 2 and 3 were used which increased the Nusselt numbers by 15.91% and 21.53% respectively at Re = 2275 with nanofluid compared to distilled water. The heat transfer performances of nanofluid was better with wire coil insert and was attributed to the effect of dispersion or back-mixing which flattens the temperature distribution and make the temperature gradient between the fluid and wall steeper.

The measured pressure loss with the use of nanofluids was almost equal to that of the distilled water. The empirical correlations developed for Nusselt number and friction factor fits with the experimental data within ±15%.

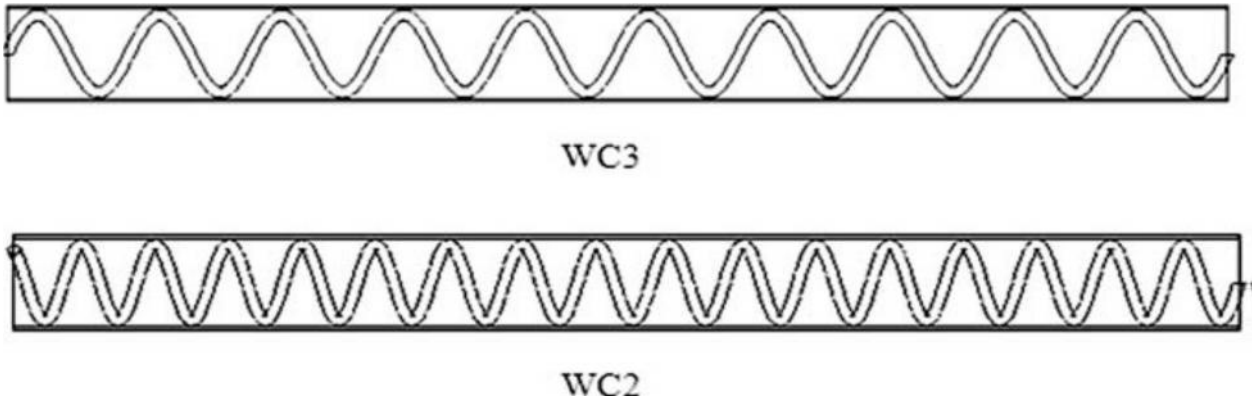

Fig. 2.5: Wire coil inserts of pitch ratio 3 (WC3) and 2 (WC2)

Syam et al. [24] had studied experimentally the turbulent convective heat transfer and friction factor behavior of Al_2O3 nanofluid in a circular tube with different aspect ratios of longitudinal strip inserts. The experiment was conducted with water and nanofluid in the range of 3000 < Re < 22,000, particle volume concentration 0 < u < 0.5% and longitudinal strip aspect ratios of 0 < AR < 18. It was found that heat transfer coefficients increase with nanofluid volume concentration and decrease with aspect ratio.

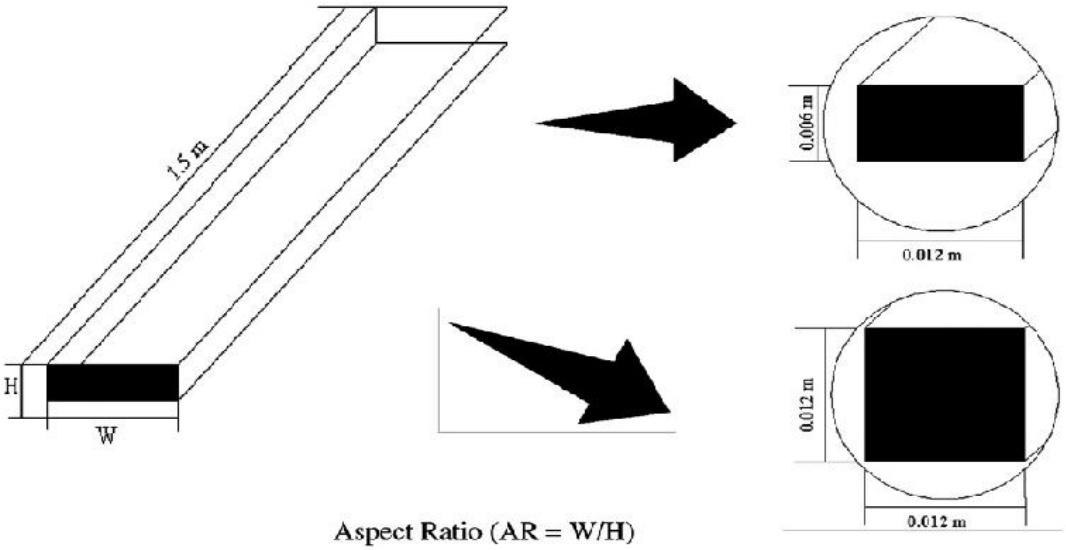

Fig. 2.6: Full-length longitudinal strip inserts.

Rashidi et al. [25] measured heat transfer coefficient of CNTs nanofluid in laminar flow regime. There was considerable enhancement in convective heat transfer coefficient of nanofluids. The increment was particularly significant in entrance length and it depended on the CNTs concentration and flow condition (Reynolds number). The enhancement in convective heat transfer was a function of axial distance from inlet and it had a decreasing trend.

Yanuar et al. [26] has investigated experimentally the flow and convective heat transfer characteristics of water-based nanofluids flowing through a spiral pipe. The test section consisted of spiral pipe with ratio pitch per diameter is 7.0 and mean hydraulic diameter of 30 mm. The straight spiral tube with 1600 mm length is used as the test section. At the inner of spiral pipe installed a circular copper pipe with 10 mm diameter. The convective heat transfer coefficient of the nanofluids increased with concentration and this enhancement was more as compared with that of pure water. The relative viscosity of nanofluids increased with an increased in concentration of nanoparticles. The Pressure drop of spiral pipe heat exchanger measured slightly as compared with circular pipe. At a given Reynolds number and nanoparticle concentration the local heat transfer coefficient of nanofluids as well as base fluid decreased with increasing axial distance from the inlet of the test section.

Heyhat et al. [27] had done experiment to determine the heat transfer coefficient and friction factor of the nanofluids flowing in a horizontal tube on fully developed region under the constant wall temperature and laminar flow condition. All physical properties of the Al_2O_3–water nanofluids, i.e. the density, specific heat capacity, thermal conductivity, and dynamic viscosity, needed to calculate the pressure drop and the convective heat transfer coefficient have been measured over a temperature range of 20–60 °C and for the nanoparticle volume fractions of 0.1%, 0.5%, 1%, 1.5%, and 2.0%, experimentally. Two correlations have been proposed for calculating the thermal conductivity and dynamic viscosity of nanofluids as a function of temperature and nanoparticle volume fraction. The results showed that the heat transfer coefficient of nanofluid was higher than that of the base fluid and increased with increasing the Reynolds number and particle concentrations. The heat transfer coefficient increased by approximately 32% in the fully developed region at 2 Vol. % nanofluids. As the volume fraction

of nanoparticles increased the pressure drop is also increased. The maximum pressure drop was about 5.7 times higher than that of pure water which occurred in the highest volume fraction of nanofluid (2%) at Reynolds number of 360.

Naraki et al. [28] investigated experimentally the overall heat transfer coefficient of CuO/water nanofluids under laminar flow regime ($100 < Re < 1000$) in a car radiator. The experimental system is quite similar to cars' cooling system. The nanofluids in all the experiments had stabilized with variation of pH and use of suitable surfactant. The results showed that the overall heat transfer coefficient with nanofluid was more than the base fluid. The overall heat transfer coefficient increased with the enhancement in the nanofluid concentration from 0 to 0.4 Vol. %. Conversely, the overall heat transfer coefficient decreased with increasing the nanofluid inlet temperature from 50 to 80 °C. With increase in volumetric flow rate over all heat transfer coefficient increased. Increasing the flow rate enhanced the overall heat transfer coefficient. According to the analysis performed using Taguchi method, the best operating conditions included minimum temperature, maximum concentration of nanofluid, maximum flow rate of nanofluid and maximum flow rate of air. The predicted maximum value for the overall heat transfer coefficient was 94.11 W/m^2 K and the error between experimental value and the predicted one was 2%. The air volumetric flow rate had 42% contribution in the overall heat transfer coefficient of CuO/water nanofluid. Nanofluid volumetric flow rate, inlet temperature and concentration of nanofluid had 23%, 22% and 13% contribution in the overall heat transfer coefficient of CuO/water nanofluid, respectively.

Jianli et al. [29] had experimentally investigated the convective heat transfer and pressure drop of dilute nanofluids containing multi-walled carbon nanotube (MWNT) in a horizontal circular tube. The suspended MWNT remarkably enhance the convective heat transfer compared with that of DI water at $Re > 100$, indicating that the enhancement in the convective heat transfer was not solely attributed to the effective thermal conductivity enhancement. The pressure drop was found to increase linearly with increasing Re, under the laminar flow condition. The corresponding friction factor for the dilute nanofluids was approximately the same as that of DI water, and could be well predicted by the Hagen-Poiseuille flow theory. The CNT nanofluids at low concentration had great potential for applications in the heat transfer systems.

Meyer et al. [30] had done experiment to determine the convective heat transfer of multi-walled carbon nanotubes flowing through a straight horizontal tube for a Reynolds number range of 1000–8000, which included the transitional flow regime. It was found that heat transfer was enhanced when comparing the data on a Reynolds–Nusselt graph but when comparing the data at the same velocity; it was shown that heat transfer was not enhanced. Pressure drop results indicated that as particle volume concentration increased, the pressure drop increased, which results from increase in viscosity. Performance evaluation of the nanofluids showed that the increase in viscosity was four times the increase in the thermal conductivity. It was concluded that the tested carbon nanofluids was not an ideal fluid for heat transfer enhancement.

Esmaeilzadeh et al. [31] had determined the hydrodynamics and heat transfer characteristics of Υ-Al_2O_3 nanoparticles inside a circular tube in laminar flow with constant heat flux. Al_2O_3/water nanofluid showed an enhanced heat transfer coefficient compared to the base fluid. There was enhancement in convective heat transfer coefficient if the particle volume fraction was increased. The heat transfer coefficient increased if heat flux was increased at a constant volume fraction, there was no significant change of friction factor for nanofluids in comparison with base fluid. A new empirical correlation was developed for Al_2O_3/water Nusselt number with maximum deviation of 15% from the experimental data.

Dongsheng et al. [32] had investigated the convective heat transfer of nanofluids at the entrance region under laminar flow conditions. The results showed considerable enhancement of convective heat transfer using the nanofluids. The enhancement increased with Reynolds number, as well as with particle concentration. It was also shown that the classical Shah equation failed to predict the heat transfer behavior of nanofluids. The enhancement decreased with axial distance and it was significant in the entrance region. The cause of enhancement was supposed to be particle migration.

References

1. M S Saterlie, H Sahin, B Kavlicoglu, Y Liu, and O.A Graeve, Surfactant Effects on Dispersion Characteristics of Copper-Based Nanofluids: A Dynamic Light Scattering Study, American Chemical Society, dx.doi: Org/10. 1021/cm203853f, Chem. Mater. 24 (2012) 3299 - 3306.
2. D anandan and K.S Rajan, Synthesis and stability of cupric-based nanofluid: A novel coolant for efficient cooling, Asian Journal of Scientific Research 5 (4) (2012) 218-227.
3. M Drzazga, M Lemanowicz, G Dzido, A Gierczycki, P.C Jako, Preparation of metal oxide-water nanofluids by two-step method, Inz. Ap. Chem. 51(5) (2012) 213-215.
4. R. S Vajjha, D. K Das and B. M Mahagaonkar, Petroleum Science and Technology, Density Measurement of Different Nanofluids and Their Comparison with Theory, 27 (2009) 612–624.
5. S Zhou and R Ni, Measurement of the specific heat capacity of water-based Al_2O_3 nanofluid, DOI: 10.1063/1.2890431.
6. L Zhou, B Wang, X.F Peng, X.Z Du, and Y.P Yang, On the Specific Heat Capacity of CuO Nanofluid, Hindawi Publishing Corporation, Advances in Mechanical Engineering, Volume 2010, Article ID 172085, 4 pages, DOI: 10.1155/2010/172085.
7. D Shin, D Banerjee, Enhanced Specific Heat of Silica Nanofluid, Journal of Heat Transfer Feburary 2011, Vol. 133 / 024501-1.
8. D Shin, D Banerjee, Enhancement of specific heat capacity of high temperature silica-nanofluids synthesized in alkali chloride salt eutectics for solar thermal-energy storage applications, International Journal of Heat and Mass Transfer, 54 (2011) 1064–1070.
9. S Halelfad, P Hstelle, B Aladag, N Doner, T Mare, Viscosity of carbon nanotubes water-based nanofluids: Influence of concentration and temperature, International Journal of Thermal Sciences, 71 (2013) 111-117.
10. P.K. Namburu, D.P. Kulkarni, A. Dandekar and D.K. Das, Experimental investigation of viscosity and specific heat of silicon dioxide nanofluids, The Institution of Engineering and Technology 2007 doi:10.1049/mnl:20070037.
11. S.M.S. Murshed, K.C. Leong, C. Yang, Enhanced thermal conductivity of TiO_2/water based nanofluids, International Journal of Thermal Sciences, 44 (2005) 367–373.

12. T Yiamsawasda, A.S Dalkilic, S Wongwises, Measurement of the thermal conductivity of titania and alumina nanofluids, Thermochimica Acta, 545 (2012) 48– 56.
13. S.M.S. Murshed, K.C. Leong, C. Yang, Investigations of thermal conductivity and viscosity of nanofluids, International Journal of Thermal Sciences, 47 (2008) 560–568.
14. L Fedele, L Colla, S Bobbo, Viscosity and thermal conductivity measurements of water-based nanofluids containing titanium oxide nanoparticles, international journal of refrigeration, 35 (2012) 1359-1366.
15. G.H Ko, K Heo, K Lee, D S Kim, C Kim, Y Sohn, M Choi, An experimental study on the pressure drop of nanofluids containing carbon nanotubes in a horizontal tube, International Journal of Heat and Mass Transfer, 50 (2007) 4749–4753.
16. L Qiang and X Yimin, Convective heat transfer and flow characteristics of Cu-water nanofluid, Science in China, (Series E) 45(4) (2002).
17. D Yulong, A Hajar, W Dongsheng, W.A Richard, Heat transfer of aqueous suspensions of carbon nanotubes (CNT nanofluids), International Journal of Heat and Mass Transfer, 49 (2006) 240–250.
18. S. Z Heris, M. N Esfahany, S. G Etemad, Experimental investigation of convective heat transfer of Al2O3/water nanofluid in circular tube International Journal of Heat and Fluid Flow, 28 (2007) 203–210
19. H Yurong, J Yi, C Haisheng, D Yulong, C Daqiang, L Huilin, Heat transfer and flow behaviour of aqueous suspensions of TiO_2 nanoparticles (nanofluids) flowing upward through a vertical pipe, International Journal of Heat and Mass Transfer 50 (2007) 2272–2281.
20. K.B. Anoop, T. Sundararajan, Sarit K. Das, Effect of particle size on the convective heat transfer in nanofluid in the developing region, International Journal of Heat and Mass Transfer 52 (2009) 2189–2195.
21. S Torii, Turbulent Heat Transfer Behavior of Nanofluid in a Circular Tube Heated under Constant Heat Flux, Hindawi Publishing Corporation, Advances in Mechanical Engineering, Volume 2010, Article ID 917612, 7 pages, doi: 10.1155/2010/917612.
22. S.M. Fotukian, M. N Esfahany, Experimental study of turbulent convective heat transfer and pressure drop of dilute CuO/water nanofluid inside a circular tube, International Communications in Heat and Mass Transfer, 37 (2010) 214–219.

23. M. Chandrasekar, S. Suresh, A. Chandra Bose, Experimental studies on heat transfer and friction factor characteristics of Al_2O_3/water nanofluid in a circular pipe under laminar flow with wire coil inserts, Experimental Thermal and Fluid Science 34 (2010) 122–130.
24. L. Syam Sundar, K.V. Sharma, Heat transfer enhancements of low volume concentration Al2O3 nanofluid and with longitudinal strip inserts in a circular tube, International Journal of Heat and Mass Transfer 53 (2010) 4280–4286.
25. F. Rashidi, N. Mosavari Nezamabad, Experimental Investigation of Convective Heat Transfer Coefficient of CNTs Nanofluid under Constant Heat Flux , Proceedings of the World Congress on Engineering, London, U.K. Vol. III WCE (2011).
26. Yanuar, N. Putra, Gunawan & M. Baqi, Flow and of convective heat transfer characteristic of spiral pipe for nanofluids, 7(3) (2011) IJRRAS_7_3_03.
27. M.M. Heyhat, F. Kowsary, A.M. Rashidi, M.H. Momenpour, A. Amrollahi, Experimental investigation of laminar convective heat transfer and pressure drop of water-based Al_2O_3 nanofluids in fully developed flow regime, Experimental Thermal and Fluid Science 44 (2013) 483–489.
28. M. Naraki, S.M. Peyghambarzadeh, S.H. Hashemabadi, Y. Vermahmoudi, Parametric study of overall heat transfer coefficient of CuO/water nanofluids in a car radiator, International Journal of Thermal Sciences, 66 (2013) 82-90.
29. J Wanga, J Zhu, X Zhang, Y Chen, Heat transfer and pressure drop of nanofluids containing carbon nanotubes in laminar flows, Experimental Thermal and Fluid Science, 44 (2013) 716–721.
30. J.P. Meyer, T.J. Mckrell, K. Grote, The influence of multi-walled carbon nanotubes on single-phase heat transfer and pressure drop characteristics in the transitional flow regime of smooth tubes, International Journal of Heat and Mass Transfer, 58 (2013) 597–609.
31. E. Esmaeilzadeh, H. Almohammadi, Sh. Nasiri Vatan, A.N. Omrani, Experimental investigation of hydrodynamics and heat transfer characteristics of Υ-Al_2O_3/water under laminar flow inside a horizontal tube, International Journal of Thermal Sciences, 63 (2013) 31-37.
32. W Dongsheng, D Yulong, Experimental investigation into convective heat transfer of nanofluids at the entrance region under laminar flow condition, International journal of heat and mass transfer 47 (2004) 5181-5188.

Chapter – 3

Preparation, stabilization and heat transfer of nanofluids

3.1 Important terms

Aggregation: Aggregation is also cluster formation, and occur due to van der Waals forces and or chemical bonding. As small particles are collided in fluid, there are chances that particles are combined to form larger particle.

Shear-thinning: A non-Newtonian fluid which exhibits higher viscosities at lower shear rates and vice-versa.

Brownian motion: The random motion of minute particles suspended in a fluid and provides a mechanism for diffusion.

Surfactant: Surfactant is a long chain hydrocarbon, consists of a hydrophobic tail portion and a hydrophilic polar head group. They are used to increase the wetability of the two materials. Surfactants are added to enhance the stability of nanofluids in the two-phase systems.

Ionic surfactant: A surfactant carrying a net charge. Surfactant is called anionic if the charge is negative and cationic if the charge is positive.

Zwitterionic surfactant: Neutral compounds having formal unit electrical charges of opposite sign.

Sedimentation: The settling of solid particles from a suspension, either naturally by gravity, or as a result of centrifugation.

Sonication: High-frequency sound waves typically used to aid the dispersion of nanoparticles in a liquid.

Hydrophilic: Tendency to dissolve or interact by water and.

Hydrophobic: Compounds that do not dissolve easily in water easily and are usually non-polar.

Chemical vapour deposition: A top-down production method where vapour is formed in a reaction chamber and condensed onto a solid substrate to form a thin film.

Zeta potential [1]

The development of a net charge at the particle surface affects the distribution of ions in the surrounding interfacial region, resulting in an increased concentration of counter ions (ions of

opposite charge to that of the particle) close to the surface. Thus there exists an electrical double layer around each particle. This development of the net charge is due to the Dipolar characteristic and ionic attribute. The electric double layer surrounding the particle consists of two layers; an **inner** layer, called the **Stern layer,** the ions in these is strongly bound and an **outer** layer, called the diffuse layer. Within the diffuse layer there are ions and particles which form a stable entity.

Ions **within** the boundary move, but any ions beyond the boundary **do not** travel with the particle. This boundary is called the **slipping plane** or surface of hydrodynamic shear. The potential that exist at the boundary is called **Zeta potential.**

The magnitude of the zeta potential gives an indication of the potential stability of the colloidal system. A colloidal system is when one of the three states of matter: gas, liquid and solid, are finely dispersed in one of the others. If there is large negative or positive zeta potential then there is tendency to repel each other and there is no tendency to flocculate. However, if zeta potential value is low then there is no force to prevent the particles coming together and flocculating. The range of zeta potential is started from ±30mV. Particles with zeta potentials more positive than +30mV or more negative than -30mV are normally considered stable.

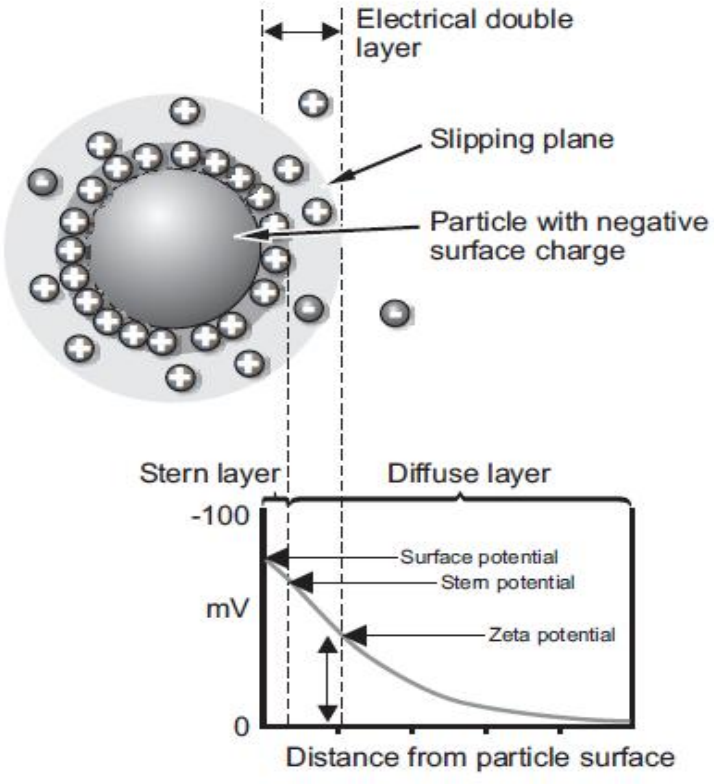

Fig. 3.1: Figure showing distribution of ions in the surrounding interfacial region

The zeta potential depends on a number of parameters, such as surface charges, ions adsorbed at the interface, and the nature and composition of the surrounding medium. The net charge in a specific medium depends on the particle charge and counter ions. The zeta potential is an index of interaction between the particles. The zeta potential is calculated according to Smoluchowski's formula,

$$\zeta = \frac{4\pi\mu}{\varepsilon} \times U \times 300 \times 300 \times 1000 \qquad (3.1)$$

Where, ζ = zeta potential in mV,

ε = dielectric constant of the medium,

μ = viscosity of solution,

U = electrophoresis mobility ($v/V/L$),

v = velocity of the particles under an electric field in cm/s,

V = applied voltage,

L = electrode distance.

PH is the most important factor that affects zeta potential.

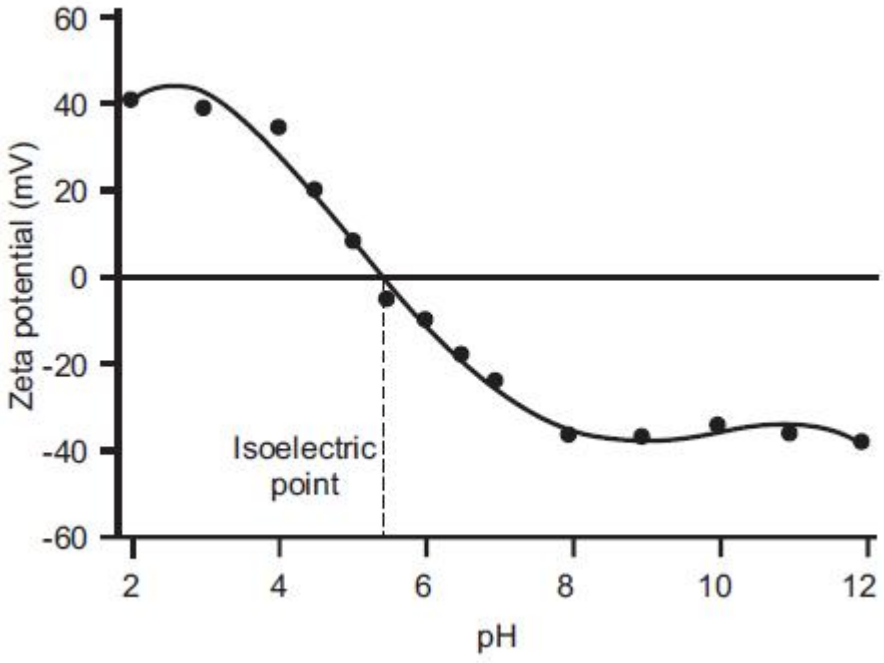

Fig. 3.2: Plot of zeta potential v/s pH.

If particle in suspension with a negative zeta potential. Particles tend to acquire a more negative charge if alkali is added to this suspension. Negative charge is neutralized if acid is added to this suspension a point will be reached where there is any further addition of acid can cause a build-up of positive charge. Therefore a positive curve is obtain when plot between zeta potential a pH and lower or negative curve obtain when plot between zeta potential at high pH.

Isoelectric point is a point where the plot is passed through zero zeta potential and is very important from a practical consideration. It is normally the point where the colloidal system is least stable.

There are two techniques/methods for measuring zeta potential:

1. Traditional method also called Micro-electrophoresis method**.** It is a based on light scattering by particles.
2. Modern methods are based on electro-acoustic methods that rely on electro-kinetic properties.

Thermophoresis

The phenomenon is observed when there is mixture of two or more types of mobile particles is subjected to the force of a temperature gradient. The phenomenon is most significant in a natural convection process, where the flow is driven by buoyancy and temperature. The particles travel in the direction of decreasing temperature. As the bulk density decreased rate of heat transfer increases.

A number of studies, such as those by Talbot et al. [2] and Yamamoto and Ishihara [3], explained and analyzed this phenomenon. The thermophoric force on a particle is given by

$$FT = \frac{6\pi\mu^2 Cs(Kr + 2.18Kr)}{\rho(1 + 3 \times 1.14Kr)(1 + 2Kr + 4.36Kr)} \frac{1}{mpT} \frac{\partial T}{\partial x} \tag{3.2}$$

This equation can be written in diffusion like form as

$$FT = -DT \frac{1}{mp} \frac{\partial T}{\partial x} \tag{3.3}$$

Where, D_T is the thermophoric diffusion coefficient, m_p the mass of the particle, Kr the ratio of the thermal conductivity of the fluid and particle, Cs=1.17, and μ is the fluid viscosity. However,

this equation is derived for the suspension of solid particles in ideal gases, a modification may be necessary to use it for solid–liquid suspensions such as nanofluids.

3.2 Preparation of nanoparticles

There are two methods for the preparation of nanoparticles:

1. Physical processes
2. Chemical processes

Typical physical methods include inert-gas condensation (IGC) developed by Granqvist and Buhrman (1976), and mechanical grinding. Chemical methods include chemical vapor deposition (CVD), chemical precipitation, micro emulsions, thermal spray, and spray pyrolysis. The current processes for making metal nanoparticles include IGC, mechanical milling, chemical precipitation, thermal spray, and spray pyrolysis. The nanoparticles prepared from the above processes are produce in the form of powders and for obtaining the nanofluids, the powder form nanoparticles are dispersed in the base fluids.

3.3 Preparation of nanofluids

There are mainly two techniques used to produce nanofluids:

1. Single-step method
2. Two-step method.

3.3.1 Single-step method

One-step technique combines the production of nanoparticles and dispersion of nanoparticles in the base fluid into a single step. Nanoparticles are directly prepared by physical vapor deposition (PVD) technique or a liquid chemical method (condensing nanophase powders from the vapor phase directly into a flowing low-vapor–pressure fluid is called VEROS method). In this method drying, storage, transportation, and dispersion of nanoparticles are avoided, so the agglomeration of nanoparticles is minimized and the stability of the nanofluids is increased [4, 5 & 6].

3.3.1.1 Disadvantage

1. They are not proper for mass production, which limits their commercialization,
2. It is applicable only for low vapor pressure host fluids.

3.3.2 Two-step method

Two-step method is the most widely used method for preparing nanofluids. It consists of two steps, in the first step nanoparticles, nanofibers or nanotubes are first produced as a dry powder by inert gas condensation, chemical vapor deposition, mechanical alloying or other suitable techniques, and in the second step nanosized powder are then dispersed into a base fluid. It is the most economic method to produce nanofluids in large scale, because nanopowder synthesis techniques have already been scaled up to industrial production levels. Due to the high surface area and surface activity, nanoparticles have the tendency to aggregate. Clustering or aggregation is the main disadvantage of the two-step method. Techniques such as intensive magnetic force agitation, ultrasonic agitation, high-shear mixing, homogenizing, and ball milling are used to minimize the particle aggregation and surfactants are added to improve the nanofluid dispersion or colloidal stability **[**4, 7, 8 & 9].

3.4 The stability evaluation methods for nanofluids

Nanofluids are a colloidal mixture of nanoparticle and the base/host fluids. Due to high specific surface area nanoparticles tend to aggregate with the time elapsed. The agglomeration of nanoparticles results in not only the settlement and clogging of micro-channels but also the decreasing of thermal conductivity of nanofluids. So the investigation on stability is also a key issue that influenced the properties of nanofluids for application [10].

3.4.1 Sedimentation method

It is the simplest and reliable method [11 & 12]. The sediment weight or the sediment volume of nanoparticles in a nanofluid under an external force field is an indication of the stability of the characterized nanofluid. The variation of concentration or particle size of supernatant particle with sediment time can be obtained by special apparatus [13]. The nanofluids are considered to

be stable when the concentration or particle size of supernatant particles keeps constant. Sedimentation photograph of nanofluids in test tubes taken by a camera is also a usual method for observing the stability of nanofluids. For the sedimentation method, long period for observation is the defect.

3.4.2 Spectral absorbency analysis

Spectral absorbency analysis is another efficient way to evaluate the stability of nanofluids. In general, there is a linear relationship between the absorbency intensity and the concentration of nanoparticles in fluid. Huang et al. evaluated the dispersion characteristics of alumina and copper suspensions using the conventional sedimentation method with the help of absorbency analysis by using a spectrophotometer after the suspensions deposited for 24 h [14].

If the nanomaterials dispersed in fluids have characteristic absorption bands in the wavelength 190–1100 nm, it is an easy and reliable method to evaluate the stability of nanofluids using UV-vis spectral analysis. The variation of supernatant particle concentration of nanofluids with sediment time can be obtained by the measurement of absorption of nanofluids, because there is a linear relation between the supernatant nanoparticle concentration and the absorbance of suspended particles. The outstanding advantage comparing to other methods is that UV-vis spectral analysis can present the quantitative concentration of nanofluids.

3.5 Thermal conductivity

Thermal conductivity is the quantity of heat that will flow through a unit area of a substance in unit time under a unit temperature gradient. The thermal conductivity is a measure of the capacity of a medium to conduct heat and it is always positive. The thermal conductivity of nanofluids depends on various parameters that including the thermal conductivities of the base fluid and the nanoparticles, the surface area, the volume fraction, the temperature, and the shape of the nanoparticles. There are no theoretical formulas currently available to predict the thermal conductivity of nanofluids convincingly.

3.6 Thermal conductivity enhancement mechanism

Recently, many theoretical studies were made and several mechanisms were proposed in order to explain the reasons for the anomalous increase of the thermal conductivity in nanofluids.

3.6.1 Brownian motion

It is defined as a random movement exhibited by a small particles suspended in a base fluid. This random movement means the collision of the small particles with one another and with the molecules of base fluid. The particles impact upon the other particles is negligible because the concentration of the particles in the nanofluids is normally low. The particles impact to molecules of base fluid is important. The forces like Van Der Waal`s forces, the stochastic forces, the electrostatic forces resulting from the electric double layer at the particle surface gives rise to the Brownian motion of particles and the hydrodynamic forces. Out of the forces electrostatic forces and the stochastic forces are only significant for small particles, whereas the van der waal`s forces are high when the distance between the particles is small. The kinetic energy transfer when particle strikes. As increase in the bulk viscosity the Brownian motion decreases with but increases with temperature. Brownian motion is best described mathematically from the Einstien- Strokes`s equation:

$$D_B = \frac{k_B T}{3\pi\mu d_p} \tag{3.4}$$

Where, D_B = Brownian Diffusion coefficient,

k_B = Boltzmann constant,

μ = viscosity of the fluid,

d_p= particle diameter

3.6.2 Clustering

Clustering is the formation of larger particles through aggregation of nanoparticles. Experimentally it was found that the size of the cluster increases with time and thus stability of nanofluids is decreases with time. Keblinski et al. [16] observed that the thermal conductivity increased as clustering in nanofluid increased. There is enhancement of thermal conductivity due to clustering of the particles due to the formation of the **particle rich** zone which has lesser thermal resistance to heat flow when compared to a **particle free** zone. On the other hand,

nanoclusters due to larger mass are likely to settle, creating a “particle-free” zone that may decrease the thermal transport. Thus, clustering of nanoparticles may have both positive and negative impact on nanofluid thermal conductivity. It is believed that the clustering of nanoparticles may occur more actively in nanofluids with higher concentration. This is because the inter-particle distance between the particles becomes smaller, which increases the probability of agglomeration due to van der Waals attraction.

3.6.3 Liquid inter-facial layering

The liquid molecules close to the particles form an ordered layer of solid-like structure known as a nanolayer. Keblinski et al. [16] suggested that as the alignment of the liquid molecules inside the solid-like interfacial nanolayer is more ordered than that of bulk liquid, nanolayer can act as a thermal bridge between a solid nanoparticle and a bulk liquid, leading to an increase in thermal conductivity of nanofluids. On the other hand, the resistance offered by these layers may pose a barrier to heat flow that might inhibit the benefit of adding highly conductive nanoparticles. This interfacial resistance is known as Kapitza resistance. In a solid/solid interface, due to imperfect contact between the solid particles at the interface, the interface layer acts as a barrier to heat transfer and thus lowers the overall effective thermal conductivity. However, in a solid/liquid interface, the contact between them could be better compared with the solid/solid interface. Hence, Kapitza resistance may not be dominant. The calculation of the Kapitza resistance per unit area by Jang and Choi [17] has revealed that it was on the order of 10−7. Hence, it seems that the nanolayer cannot act as a barrier to heat transfer.

3.7 Convection heat transfer

Convection is as mode of heat transfer. In convection heat transfer occurs between a surface and moving medium, when they are at different temperatures. It comprises of two mechanisms. First is transfer of energy due to random molecular motion (diffusion) and second is the energy transfer by bulk or macroscopic motion of the fluid (advection). It consists of conduction from surface to adjacent layer of fluid + energy transfer due to mass transfer + conduction to adjacent layer of fluid to receiving surface.

It is generally of two types:

1. Forced convection
2. Natural convection

In Forced convection the fluid flow is caused by some external agent such as pump, fan and compressor over the plates or through the pipes or ducts. In Natural or Free convection the fluid flow is caused by virtue of the natural difference in densities of hot and cold fluids. The denser portion of the fluid moves downward because of the greater force of gravity, as compared with the force on the less dense

Convection heat transfer strongly depends upon fluid properties, dynamic viscosity, thermal conductivity *k*, density ρ, specific heat Cp and fluid velocity. It also depends upon type of fluid flow, geometry and roughness of the solid surface

There are many methods for increasing the heat transfer in processes. The flow of heat in a process can be calculated by Newton`s law of cooling that is:

$$Q = h\ A\ \Delta T \tag{3.5}$$

Where Q is the heat flow, h is the heat transfer coefficient, A is the heat transfer area, and ΔT is the temperature difference

From the above equation it is clear that heat transfer is increased by:

1. increasing ΔT
2. increasing A
3. increasing h
4. Heat transfer increases by increasing the temperature difference ΔT, but ΔT is increases up to certain limit due to material constraints. Maximizing the heat transfer area A also increases heat transfer like in Heat exchanger but it also has limitation like limited space, weight etc. heat transfer also increases by increasing the heat transfer coefficient by using more efficient heat transfer methods, or by improving the transport properties of the heat transfer material
5. Heat transfer coefficient can be increased by two methods. First method: h is a function of Reynolds number and Reynolds number depends directly upon velocity. Thus if velocity increases h also increases. This method has limitation, on increasing velocity friction losses also increases (frictional losses= f (V^2)). Second method: as we know that Nusselt number (Nu) = h d/k_f. Where, k_f is the fluid conductivity and d is the diameter if fluid is flowing through the pipe. On rearranging above formulae we get h = Nu k_f/d. i.e h

is directly proportional to kf. Which means h is increased by increasing the thermal conductivity of the fluids for a given Nusselt number. The thermal conductivity of the fluids improves by incorporating the solid particles.

3.8 Dimensionless parameter in convection

1. **Reynolds number:** It is defined as the ratio of inertia force to the viscous force.

$$\mathrm{Re} = \frac{\text{inerta force}}{\text{viscous force}} = \frac{°uL}{«} \tag{3.6}$$

It determines whether the flow is laminar or turbulent.

2. **Prandtl number:** It is define as the ratio of momentum diffusivity to the thermal diffusivity.

$$\mathrm{Pr} = \frac{\text{Momentum diffusivity}}{\text{Thermal diffusivity}} = \frac{¬}{\sim} = \frac{«C_p}{k} \tag{3.7}$$

It indicates the relative efficiency of momentum and heat transfer.

Generally

$$\frac{¢}{¢_t} = \mathrm{Pr}^n \qquad \text{Where n > 0} \tag{3.8}$$

For Prandtl number Pr = 1, the velocity and the thermal boundary layers will be of same thickness

3. **Nusselt number :** It is the ratio of the convective to the conductive heat flux

$$Nu = \frac{\text{convective heat flux}}{\text{conductive heat flux}} = \frac{h\Delta T}{k\Delta T / L} = \frac{hL}{k} \tag{3.9}$$

4. **Grashof number:** It is the ratio of the product of Inertia force and Buoyancy force to the square of viscous force.

$$Gr = \frac{(\text{inertia force}) \times (\text{buoyancy})}{(\text{viscous force})^2} = \frac{(\ Y\Delta T) \times L^3}{¬^2} \tag{3.10}$$

It determines whether the flow is laminar or turbulent in natural convection.

References

1. Malvern Zeta potential - An introduction in 30 minutes MRK654-01.pdf
2. L Talbot, R.K. Cheng, R.W. Schefer, and D. R. Willis. Thermophoresis of particles in heated boundary layer, Journal of Fluid Mechanics, 101 (1980) 737–758.
3. K Yamamoto, and Y. Ishihara, Thermophoresis of spherical particle in a rarefied gas of a transition regime, Phys. Fluids, 31 (1988) 3618–3624.
4. S.K. Das, S.U.S. Choi, W.H. Yu, T. Pradeep, nanofluid: Science and Technology, John Wiley & Sons Inc., 2007.
5. X.Q Wang, A.S Mujumdar, Heat transfer characteristics of nanofluids: a review, International Journal of Thermal Science, 46 (1) (2007) 1–19.
6. Y. Li, J.E Zhou, S. Tung, E. Schneider, S. Xi, A review on development of nanofluid preparation and characterization, Powder Technology, 196 (2) (2009) 89–101.
7. W Yu, D France, J. L Routbort, and S. U. S Choi, Review and Comparison of Nanofluid Thermal Conductivity and Heat Transfer Enhancements, Heat Transfer Engineering, 29(5) (2008) 432-460.
8. J. M Romano, J. C Parker, and Q. B Ford, Application Opportunities for Nanoparticles Made from the Condensation of Physical Vapors, Adv. Pm. Part., (1997) 12-13.
9. Y Li, J Zhou, S Tung, E Schneider, S Xi, A review on development of nanofluid preparation and characterization, Powder Technology, 196 (2009) 89–101.
10. W Yu and H Xie, A Review on Nanofluids: Preparation, Stability Mechanisms, and Applications, Hindawi Publishing Corporation Journal of Nanomaterials Volume 2012, Article ID 435873, 17 pages doi:10.1155/2012/435873.
11. X. Wei and L. Wang, Synthesis and thermal conductivity of microfluidic copper nanofluids, Particuology, 8(3) (2010) 262–271.
12. X. Li, D. Zhu, and X. Wang, Evaluation on dispersion behavior of the aqueous copper nano-suspensions, Journal of Colloid and Interface Science, 310(2) (2007) 456–463.
13. Y. Li, J. Zhou, S. Tung, E. Schneider, and S. Xi, A review on development of nanofluid preparation and characterization, Powder Technology, 196(2) (2009) 89–101.

14. J. Huang, X. Wang, Q. Long, X. Wen, Y. Zhou, and L. Li, Influence of pH on the stability characteristics of nanofluids, Proceedings of the Symposium on Photonics and Optoelectronics (SOPO ’09) 2009.
15. S.P Jang and S.U.S Choi, Role of Brownian Motion in the Enhanced Thermal Conductivity of the Nanofluids, Applied physics Letter, May(2004)
16. P Keblinski, , S. R Phillpot, S. U. S Choi, and Eastman, J. A., Mechanism of Heat Flow in Suspension of Nano-Sized Particles (Nanofluids), International Journal of Heat and Mass Transfer, 45 (2002) 855–863.
17. S. P Jangand S. U. S Choi, Effects of Various Parameters on Nanofluid Thermal Conductivity, Journal of Heat Transfer, 129 (2007) 618–623.

Chapter-4

Experimental Work and Set-up Description

4.1 Objectives

1. To determine the heat transfer characteristic of CuO-distilled water nanofluid flowing through a circular pipe.
2. To determine the pressure drop along the length of the test section.

4.2 Preparation of nanofluids

The copper oxide (CuO) nanoparticles of average size 40nm were purchased from Intelligent Materials Pvt. Ltd, Panchkula. TEM analysis of CuO nanoparticles is shown in fig. 4.1. The properties of CuO nanoparticles are given in table 4.1.

Table 4.1: Properties of the copper oxide nanoparticles [1]

Chemical Name	CuO nanopowder
Appearance	Black powder
Purity	>99%
Average particle size	40nm
P^H	7
Density (kg/m^3)	6400
Specific heat (J/kg.K)	535
Thermal conductivity (W/m.K)	69

The distilled water and sodium dodecyl sulphate surfactant were obtained from the chemical engineering Department. The preparation of the nanofluid is the first step for this heat transfer

experiment. The nanofluid was prepared by the two-step method in which the nanoparticles were dispersed in the base fluid. First of all calculation was made for the weight of CuO nanoparticles

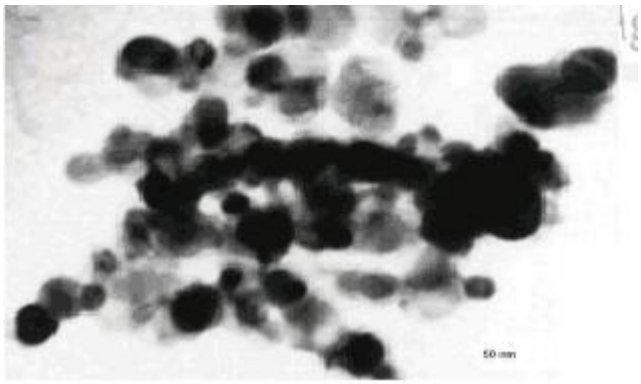

Fig. 4.1: TEM analysis of CuO nanoparticles

used for 50ml of the distilled water for different concentration. It was 0.32gm, 0.8gm and 1.6gm for 0.1 Vol. %, 0.25 Vol. % and 0.5 Vol. %, respectively of the nanofluid. The mass of the SDS surfactant used, was 0.1gm for the 50ml distilled water and for all the three concentration. After the calculation of the mass of the CuO nanoparticles and the SDS surfactant, the required mass of the SDS was directly added to the distilled water and thoroughly stirred. Then required mass of the CuO was added to the surfactant dissolved distilled water and then stirred thoroughly [2]. To increase the dispersion stability the sonication was done by the ultra-sonicator water bath for three hours. After the sonication the prepared nanofluids were used to measure the thermo-physical properties. A fresh nanofluid was prepared every time when it was used in experimental set-up for taking the readings. The three prepared sample are shown below in fig. 4.2.

Fig. 4.2: Copper oxide distilled water based nanofluids (0.1 Vol. %, 0.25 Vol. % & 0.50 Vol. %)

4.2.1 Sodium dodecyl sulphate

The Sodium dodecyl sulphate is the chief surfactant of the Sodium lauryl sulphate group. Its molecular weight is 238.38. It is an anionic surfactant, which will decrease hydrophobicity and can participate in charge stabilization of the suspension. By lowering the surface tension of aqueous solutions, surfactants can act as wetting agents by enhancing the spread of water over surfaces. The structure of SDS is shown below in fig. 4.3.

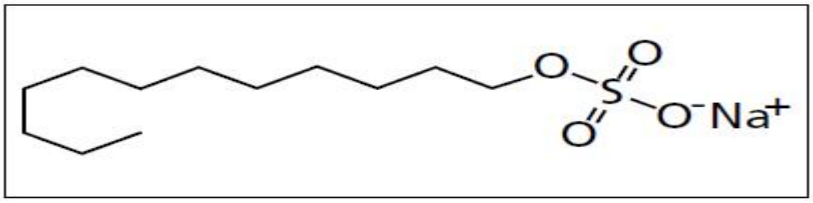

Fig. 4.3: Structure of the SDS

4.3 Description of the Experimental set-up

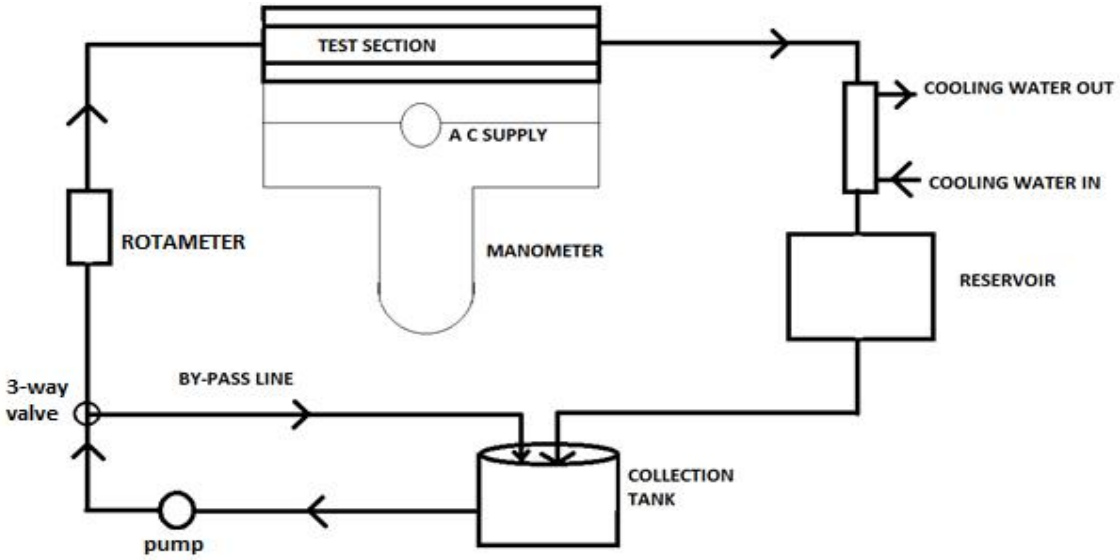

Fig. 4.4: Experimental Set-up

The experimental set-up for measuring the convective heat transfer coefficient and pressure drop is shown schematically in Fig. 4.4. Fig. 4.5 shows the actual picture of the experimental set-up

Fig. 4.5: picture of the experimental set-up

4.3.1 Test section

The test section was a straight copper pipe outer diameter ½ inch (12.7 mm), inner diameter 0.0095m, length 1.5 meter, embedded with 8 Temperature sensor, 6 on surface, 1 each at inlet & outlet with manometer for pressure difference across test length. The test section is electrically heated by an adjustable AC power supply. A nickel-chrome wire heater of 250 watts is wrapped over the test piece with varied for controlled external heating of section. An AC power supply is used as a power source to the heater. There is a thick thermal isolating layer surrounding the heater along the test section [5, 6].

4.3.2 Differential u-tube manometer

Differential manometers are the devices used for measuring the difference of pressure between two points in a pipe or two different pipes. A differential manometer consists of a U-tube, containing a heavy liquid, whose two ends are connected to the points, whose difference of pressure is to be measured. If one end of the tube is in a place with higher air or fluid pressure, the pressure will push down the liquid on that side of the tube. By measuring the difference

between the heights of liquid, it is possible to calculate the difference in pressure. The differential U-tube manometer is shown in fig. 4.6. The fluid used was water.

Fig. 4.6: U-tube differential manometer

4.3.3 Double-pipe heat exchanger

Heat exchangers are practical devices used to transfer energy from one fluid to another. However, they are not only used in heating applications, such as space heaters, but are also used in cooling applications, such as refrigerators and air conditioners. Many types of heat exchangers can be distinguished from on another based on the direction the liquids flow.

The double-pipe heat exchanger is one of the simplest types of heat exchangers. It is called a double-pipe exchanger because one fluid flows inside a small diameter pipe and the other fluid flows through the annular space between the two pipes. This is a concentric tube construction. Flow in a double-pipe heat exchanger can be parallel flow or counter flow. In parallel flow arrangement the flow of the two streams is in the same direction while in counter flow arrangement the flow of the streams is in opposite directions. Counter flow heat exchangers tend to be more effective than other types of exchangers. Double-pipe heat exchanger is shown in fig. 4.7.

Fig. 4.7: Double-pipe heat exchanger

4.3.4 Collection tank

Collection tank was made of stainless steel insulated with ceramic fiber wool. It was used for collecting the nanofluids and pump was placed in it.

4.3.5 Pump

A pump is a mechanical device used to displace fluid. It is used to increase the pressure of a liquid, adding energy to the hydraulic system, to move the fluid of a zone of smaller pressure or altitude to another one of greater pressure or altitude. The pump transforms the mechanical energy into hydraulic energy of the incompressible fluid and exerts work on a liquid. The picture of the pump used is shown in fig. 4.8. The specification of the pump is shown in table 4.2.

Fig. 4.8: Pump

Specification of Pump:

Table 4.2: Specification of pump

Power consumption	18W
Voltage	AC 220V, 50Hz
Outlet nozzle size	½ inch or 12.7mm
Maximum head	1.5m or (5 Ft.)
Maximum flow	750 L/H
Maximum cooler Height	1.2m or (4 Ft.)

4.3.6 Rotameter

Rotameter is a particular kind of flowmeter, based on the variable area principle. They provide a simple, precise and economical means of indicating the rate of flow of the fluids. This variable area principle consists of three basic elements: A uniformly tapered flow tube, a float, and a measurement scale. A control valve may be added if flow control is also desired. In operation, the rotameter is positioned vertically in the fluid system with the smallest diameter end of the tapered flow tube at the bottom. This is the fluid inlet. The float, typically spherical, is located inside the flow tube, and is engineered so that its diameter is nearly identical to the flow tube's inlet diameter.

When fluid (gas or liquid) is introduced into the tube, the float is lifted from its initial position at the inlet, allowing the fluid to pass between it and the tube wall. As the float rises, more and more fluid flows by the float because the tapered tube's diameter is increasing. Ultimately, a point is reached where the flow area is large enough to allow the entire volume of the fluid to flow past the float. This flow area is called the annular passage. The float is now stationary at that level within the tube as its weight is being supported by the fluid forces which caused it to rise. This position corresponds to a point on the tube's measurement scale and provides an indication of the fluid's flow rate. The picture of the rotameter used is shown in fig. 4.9.

Fig. 4.9: Rotameter

4.3.7 RTD Pt 100 Thermocouple

RTD stand for resistive temperature device which produce a change in resistance to other material of thermocouple correspond to a variation in temperature. Pt is the chemical symbol for platinum, 100 is the resistance in ohm of the platinum at 0°C. The resistance changes approximately linearly with temperatures and it are 0.385 ohm/°C. So, by measuring the resistance we can calculate the temperature. RTD is also called the platinum film temperature detector. Platinum is used most commonly due to purity and consistency/predictability (linear R vs. T). The picture of the thermocouple used is shown in fig. 4.10.

The principle of operation is to measure the resistance of a platinum element. The most common type (PT100) has a resistance of 100 ohms at 0 °C and 138.4 ohms at 100 °C. There are also PT1000 sensors that have a resistance of 1000 ohms at 0 °C**)**. It offers excellent accuracy over a wide temperature range (from-200 to +850 °C).

Fig. 4.10: Thermocouple

4.4 Instruments used

4.4.1 Ultra sonicator water bath

Sonication is the act of applying sound (usually ultrasound) energy to agitate particles in a sample, for various purposes. In the laboratory, it is usually applied using an ultrasonic bath known as a sonicator. Sonication can be used to speed dissolution, by breaking intermolecular interactions. Sonication is commonly used in nanotechnology for evenly dispersing nanoparticles in liquids [7, 8]. Ultra sonicator water bath is shown in fig. 4.11.

Fig. 4.11: Ultra-sonicator water bath

4.4.2 Pycnometer

A pycnometer is used for measuring the density of the solutions. The pycnometer comes from the Greek puknos, meaning “density”, also called pycnometer or specific gravity bottle. The picture of the pycnometer is shown in fig. 4.12.

Fig. 4.12: Pycnometer

It is a very precise method. It uses a working liquid with well-known density, such as water. We will use distilled water, for which temperature dependent values of density is known. The pycnometer is a glass flask with a close-fitting ground glass stopper with a capillary hole through it. This fine hole releases a spare liquid after closing a top-filled pycnometer and allows for obtaining a given volume of measured and/or working liquid with a high accuracy [9].

First of all, weigh the empty pycnometer with digital weighing balance machine. Then, fill the pycnometer with distilled water. The volume of distilled water that is filling the pycnometer and the stopper is:

$$V = \frac{m_{water}}{\rho_{water}} \tag{4.1}$$

Where m_{water} is experimentally determined weight of water (empty pycnometer weight subtracted). We repeat the procedure for the liquid with unknown density ρ_L and determine its weight m_L (measured weight minus weight of empty pycnometer). Volume V obtained in this measurement is the same as the volume of water determined from equation 4.1. It follows alternated equation:

$$V = \frac{m_L}{\rho_L} \tag{4.2}$$

Combining equations (3.5) and (3.6)

$$\frac{m_{water}}{\rho_{water}} = \frac{m_L}{\rho_L} \tag{4.3}$$

This yields a relation that provides the density of measured liquid

$$\rho_L = \frac{m_L}{m_{water}} \bullet \rho_{water} \tag{4.4}$$

Before doing any measurement, first of all, pycnometer is to be filled with potassium dichromate solution for at least 12 hours. As potassium dichromate solution is good cleaning agent. So, it removes any kind of dust particles in the pycnometer. Then, it is cleaned with distilled water, and

then it is to be dried in Oven at above 120 °C for at least 4-5 hours. So, that no water was left in it. Now, it is ready to use [7, 8].

Now, First of all, weigh the empty pycnometer with the digital weighing balance machine. Then pour the exactly 5 ml sample of nanofluid in the pycnometer by micro pipette. Then weigh the pycnometer again. Now this will give the weight of 5 ml sample of nanofluid sample by subtracting the empty pycnometer weight from the total weight. Fig. 4.13 shows digital weighing balance machine.

Fig. 4.13: Digital weighing balance machine

So, density of this 5 ml sample can be found by the following equation:

$$\rho = \frac{\text{weight of nanofluid sample in gm}}{5\text{ml}} = ---- \text{gm/cm}^3 \qquad (4.5)$$

The above procedure is for density measurement by pycnometer at room temperature. But for different temperature, we use hot plate as shown in Fig. 4.14 magnetic stirrer with hot plate

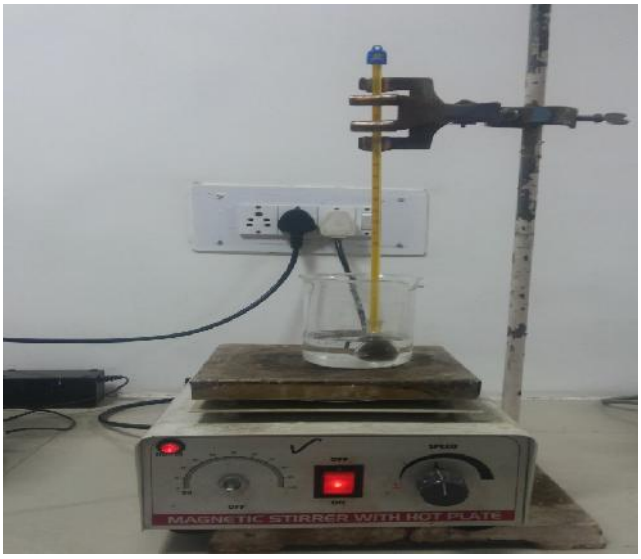

Fig. 4.14: Magnetic stirrer with hot plate

We taken a beaker, and filled the water in it up to the height a little less than the height of pycnometer. Put this beaker on the hot plate. This worked as a hot water bath for pycnometer. Also with the help of a clamp and stand, put a thermometer in the beaker for different temperature measurement. Now very gently put the pycnometer filled with nanofluid inside the beaker and then slowly increased the temperature of the hot plate. This whole arrangement is shown in Fig. 412. Now repeat it, at every temperature and then weigh the pycnometer on digital weighing balance machine [7, 8]. And the density of nanofluid sample can be found out by equation 4.5.

4.4.3 Thermal properties analyzer KD2 PRO [10]

The KD2 Pro is a hand held device used to measure thermal properties. It consists of handheld controller and sensors that can be inserted into the medium. The single-needle sensors measure thermal conductivity and resistivity; while the dual-needle sensor also measures volumetric specific heat capacity and diffusivity. KD2 PRO shown in fig. 4.15.

Fig. 4.15: KD2 PRO

Specifications:

Table 4.3: Specification of Thermal properties analyzer KD2 PRO

Controller	-50 to +150 °C
Power	4 AA cells
Battery life	At least 500 readings in constant use or 3 years with no use (battery drain in sleep mode < 50 μA)
Case size	15.5 cm x 9.5 cm x 3.5 cm
Display	3 cm x 6 cm, 128 x 64 pixel graphics LCD
Keypad	6 key, sealed membranes
Data storage	4095 measurements in flash memory (both raw and processed data are stored for download)
Interface	9-pin serial
Read modes	Manual and Auto Read

4.4.3.1 Sensors:

4.4.3.1.1 Single-needle (KS-1) 60 mm (small):

This single needle KS-1 sensor measures thermal conductivity and thermal resistivity. It is designed primarily for liquid samples and insulating materials (thermal conductivity < 0.1 W/

(m.K)). It is shown in fig. 4.16. The KS-1 sensor applies a very small amount of heat to the needle which helps to prevent free convection in liquid samples. However, the small size of the needle and typically short heating time make the KS-1 a poor choice for granular samples such as soil and powders where contact resistance can be an important source of error. In insulating materials, the errors from contact resistance become negligible making the KS-1 sensor a good choice.

Fig. 4.16: Single-needle (KS-1)

Specification:

Table 4.4: Specification single-needle (KS-1)

Size	1.3 mm diameter x 60 mm long
Range	0.02 to 2.00 W/(m· K) (thermal conductivity) 50 to 5000 °C-cm/W (thermal resistivity)
Accuracy (Conductivity)	± 5% from 0.2 - 2 W/(m· K) ±0.01 W/(m· K) from 0.02 - 0.2 W/(m· K)
Cable length	0.8m

4.4.3.1.2 Single-needle (TR-1) 100 mm (large):

The large single needle TR-1 sensor measures thermal conductivity and thermal resistivity. It is designed primarily for soil, concrete, rock, and other granular or solid materials. The relatively large diameter and typically longer heating time of the TR-1 sensor minimize errors from contact resistance in granular samples or solid samples with pilot holes. The TR-1 needle heats the

sample significantly more than the KS-1 sensor, which allows it to measure higher thermal conductivity samples, but means that you not measure liquid samples with the TR-1 sensor. The large diameter of the TR-1 is more robust than the KS-1, meaning that it is less likely to be damaged by normal usage conditions in soil or other solid materials. Additionally, the dimensions of the TR-1 sensor conform to the specifications for the Lab Probe called out by the IEEE 442-03 Guide for soil Thermal resistivity measurements. The TR_1 needle is shown in fig. 4.17.

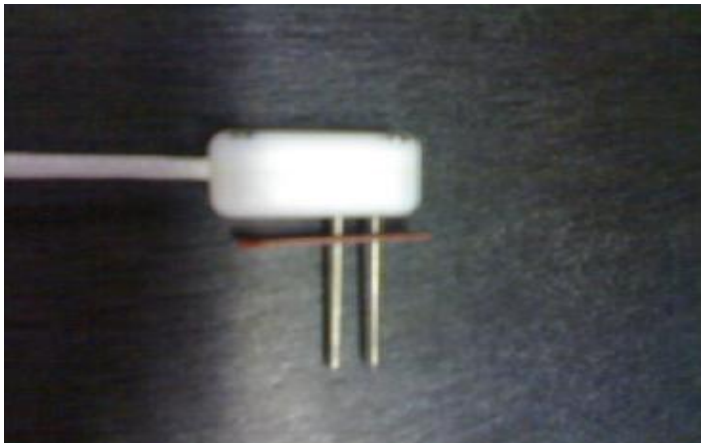

Fig. 4.17: Single-needle (TR-1)

Specification:

Table 4.5: Specification single-needle (TR-1)

Size	2.4 mm diameter x 100 mm long
Range	0.10 to 4.00 W/(m. K) (thermal conductivity) 25 to 1000 °C.cm/W (thermal resistivity)
Accuracy (Conductivity)	±10% from 0.2 - 4 W/(m. K) ±0.02 W/(m. K) from 0.1 - 0.2 W/(m. K)
Cable length	0.8m

4.4.3.1.3 Dual-needle (SH-1) 30 mm:

This dual needle SH-1 sensor measures volumetric heat capacity, thermal diffusivity, thermal conductivity, and thermal resistivity. The SH-1 is compatible with most solid and granular materials, but should not be used in liquids due to the large heat pulse and possible resulting free convection in liquid samples.

Specifications:

Table 4.6: Specifications dual-needle (SH-1)

Size	1.3 mm diameter x 30 mm long, 6 mm spacing
Range	0.02 to 2.00 W /(m- K) (thermal conductivity) 50 to 5000 °C-cm/W (thermal resistivity) 0.1 to 1 mm^2/s (diffusivity) 0.5 to 4 $mJ/(m^3K)$ (volumetric specific heat)
Accuracy (Conductivity)	± 10% from 0.2 - 2 W/(m· K) ±0.01 W/(m· K) from 0.02 - 0.2 W/(m· K)
Accuracy (Diffusivity)	±10% at conductivities above 0.1 W/(m· K)
Accuracy(Volumetric Specific Heat)	±10% at conductivities above 0.1 W/(m· K)
Cable length	0.8m

4.4.4 Brookfield DV-III Rheometer [11]

The Brookfield DV-III Programmable Rheometer measures fluid parameters of Shear Stress and Viscosity at given Shear Rates. Viscosity is a measure of a fluid's resistance to flow. The principle of operation of the DV-III is to drive a spindle (which is immersed in the test fluid) through a calibrated spring. The viscous drag of the fluid against the spindle is measured by the spring deflection. Spring deflection is measured with a rotary transducer. The measuring range of a DV-III (in centipoise) is determined by the rotational speed of the spindle, the size and shape of the spindle, the container the spindle is rotating in, and the full scale torque of the calibrated spring. It is shown in fig. 4.18.

Fig. 4.18: Brookfield LVDV-III rheometer

Specification

Table 4.7: Specification Brookfield LVDV-III rheometer

Speed Range	0-250 RPM, 0.1 RPM increments
Viscosity Accuracy	±1.0% of full scale range for a specific spindle running at a Specific speed.
Temperature sensing range	- 100°C to 300°C (-148°F to 572°F)
Temperature accuracy	±1.0°C from -100°C to 150°C ±2.0°C from +150°C to 300°C
Analog torque output	0 - 1 Volt DC (0 - 100% torque)
Analog temperature output	0- 4 Volts DC (10mV / °C)

4.5 Evaluation of heat transfer coefficient

For the calculation of the heat transfer coefficient and pressure drop, the thermo- physical properties of the CuO-Distilled water required to be calculated. As already mention that conductivity was measured with the help of KD2 PRO thermal properties analyzer, viscosity was measured with Brookfield LVDV-III Rheometer and density with pycnometer or specific gravity bottle. Specific heat was calculated by the model or equation which assumes that the base fluid and the nanoparticles are in thermal equilibrium. The equation is:

$$C_{nf} = \frac{\left(¤C_p + (1+¤)°_{bf} C_{bf}\right)}{°_{nf}} \tag{4.6}$$

Where,

C_{nf} = specific heat of the nanofluids

C_{bf} = specific heat of the base fluid

Φ = volume fraction

ρ_{bf} = density of the base fluid

ρ_{nf} = density of the nanofluids

As the test section is explained earlier, Q_1 heat supplied from the nichrome wire heater which is wrapped around the outer surface of the test section. The tube become heated which heat up the fluid flowing through it. So, Q_2 is the heat gained by the base fluid or CuO/water nanofluid which is less than the heat supplied i.e. Q_1. Some heat losses as the insulation losses. In equation form:

$$Q_1 \text{ (Heat supplied)} = V \times I \tag{4.7}$$

$$Q_2 \text{ (Heat gained)} = Q_1 \text{- Losses} \tag{4.8}$$

Which is further equals to:

$$Q_1 = mC_p \Delta T = mC_p (T_8 - T_1) \tag{4.9}$$

Where Q_1 is the heat gained by the nanofluid, *m* is the mass flow rate of nanofluid, and T_8 and T_1 are the temperatures of the nanofluid at the outlet and inlet of the test section respectively. The thermocouples are fixed at the outer section of the pipe. So reading of the temperature at the inner section is given by the conduction equation for hollow cylinder which is given below:

$$Q_1 = \frac{2\pi kL(T_{so} - T_{si})}{\ln \frac{r_o}{r_i}} \tag{4.10}$$

From above equation T_{si} can be calculated.

Where,

T_{so} = Outside avg. surface temperature of test section

$$= \frac{(T_2 + T_3 + T_4 + T + T_6 + T_7)}{6} \tag{4.11}$$

T_{si} = Inside avg. surface temperature of test section

r_o = Outside radius of the test section

r_i = Inside radius of the test section

k= thermal conductivity of test section (copper tube)

L = length of the test section

The convective heat transfer coefficient (h) is defined as:

$$h(x) = \frac{q}{(T_w(x) - T_f(x))} \tag{4.12}$$

Where, x is the axial distance from the inlet of the test section, q is the heat flux, T_w and T_f are the wall and fluid mean temperature, respectively.

And fluid mean temperature is given by the energy balance:

$$T_f = T_{in} + \frac{qPx}{(\circ AuC_p)} \tag{4.13}$$

Where, C_p is the specific heat, p is the surface perimeter $(P = \circledR D)$, D is the diameter of the test pipe, u is the average fluid velocity, A is the cross- sectional area, ρ is the fluid density.

The Nusselt number is defined as:

$$Nu(x) = \frac{h(x) \bullet D}{k} \tag{4.14}$$

Where, k is the fluid thermal conductivity.

And Nusselt number is the function of the Reynolds number and Prandtl number

$$\mathrm{Re} = \frac{(\circ uD)}{\ll} \tag{4.15}$$

$$\mathrm{Pr} = \frac{\neg}{\sim} \tag{4.16}$$

Where ν is the kinematic viscosity, μ is the dynamic viscosity and α is the fluid thermal diffusivity.

Refrences

1. Intelligent material Pvt. Ltd. www.nanoshel.com.
2. M. Naraki, S.M. Peyghambarzadeh, S.H. Hashemabadi, Y. Vermahmoudi, Parametric study of overall heat transfer coefficient of CuO/water nanofluids in a car radiator, International Journal of Thermal Sciences, 66 (2013) 82-90.
3. Product Data Sheet 739 Surfactants Bangs Laboratory, INC
4. National Industrial Chemical Notification and Assessment Scheme existing chemical information sheet.
5. W Dongsheng, D Yulong, Experimental investigation into convective heat transfer of nanofluids at the entrance region under laminar flow condition, International journal of heat and mass transfer, 47 (2004) 5181-5188.
6. H Yurong, Y Jin, C Haisheng, D Yulong, C Daqiang, L Huilin, Heat transfer and flow behaviour of aqueous suspensions of TiO_2 nanoparticles (nanofluids) flowing upward through a vertical pipe, International Journal of Heat and Mass Transfer, 50 (2007) 2272–2281.
7. D.Gangacharyulu and Harkirat, Preparation and characterization of nanofluids and some investigation in biological applications, M. Tech Thesis, T.U., Patiala (2010).
8. D.Gangacharyulu and Mahesh Juneja, Experimental investigation of thermophysical properties of nanofluids, M. Tech Thesis, T.U., Patiala (2012).
9. www.fpharm.uniba.sk/fileadmin/user_upload/english/Fyzika/Density_determination_by_pycnometer.pdf.
10. KD2 Pro Thermal Properties Analyzer, Operator's Manual (Version 10), supplied by Decagon Devices, Inc., WA 99163 USA.
11. Brookfield Digital Viscometer, Model DV-E, Operating Instructions, Manual No. M/98-350-g0307, Brookfield Engineering Laboratories, Inc., 11 Commerce Boulevard, Middleboro, MA 02346 USA.

Chapter-5

Result and discussions

5.1 Introduction

The thermo-physical properties of nanofluids are measured by various equipments such as Brookfield LVDV-III Rheometer, pycnometer or specific gravity bottle, KD2 PRO thermal property analyzer. An experimental setup was used for measuring the temperature for calculating the heat transfer coefficient and pressure drop at different flow rates and at different concentration of nanoparticles. All the results shown in form of table and graph briefly discussed in this chapter.

5.2 Density measurement

The value of weight of 5ml of distilled water (DW), 0.1 Vol. %, 0.25 Vol. % and 0.5 Vol. % of CuO-distilled water based nanofluids for temperature range 30°C to 80° C are respectively, given in Table 5.1.

Table 5.1: Weight of distilled water and CuO-distilled water based nanofluids (gm.)

S. No.	Temperature (°C)	DW	0.10 Vol. % CuO	0.25 Vol. % CuO	0.50 Vol. % CuO
1	30	4.9762	5.0226	5.0422	5.0586
2	40	4.9574	5.0101	5.0312	5.0472
3	50	4.9377	4.9978	5.0216	5.0396
4	60	4.9184	4.9792	5.0092	5.0306
5	70	4.8921	4.9553	4.9903	5.0179
6	80	4.8646	4.9339	4.9597	4.9947

Table 5.2: Density of distilled water and CuO-distilled water based nanofluids.

S. No	Temperature (°C)	Pycnometer reading Density (kg/m³)			
		DW	0.1 Vol. % CuO	0.25 Vol. % CuO	0.5 Vol. % CuO
1	30	995.23	1004.51	1008.43	1011.72
2	40	991.47	1002.03	1006.27	1009.43
3	50	987.53	999.56	1004.31	1007.92

4	60	983.67	995.84	1001.84	1006.11
5	70	978.42	991.06	998.06	1003.58
6	80	972.91	986.78	991.93	998.93

The calculated value of density of distilled water and copper oxide distilled water based nanofluids is shown in Table 5.2. It can be seen from the Fig 5.1, that at 30°C, with the increase in the concentration of nanoparticles from 0.1 Vol. % to 0.50 Vol. %, density of copper oxide-distilled water based nanofluids increases from 0.93 % to 1.66 % (i.e. 0.93 % for 0.1 Vol. % concentration, 1.33 % for 0.25 Vol. % concentration, 1.66 % for 0.50 Vol. %) compared to base fluid i.e. distilled water.

And with the increase in temperature, density of distilled water and copper-oxide distilled water based nanofluids decreases. From 30°C to 80°C, density decreases by 2.24 % for distilled water, 1.77 % for 0.1 Vol. % concentrations, 1.64 % for 0.25 Vol. % concentrations, and 1.26 % for 0.50 Vol. % concentrations.

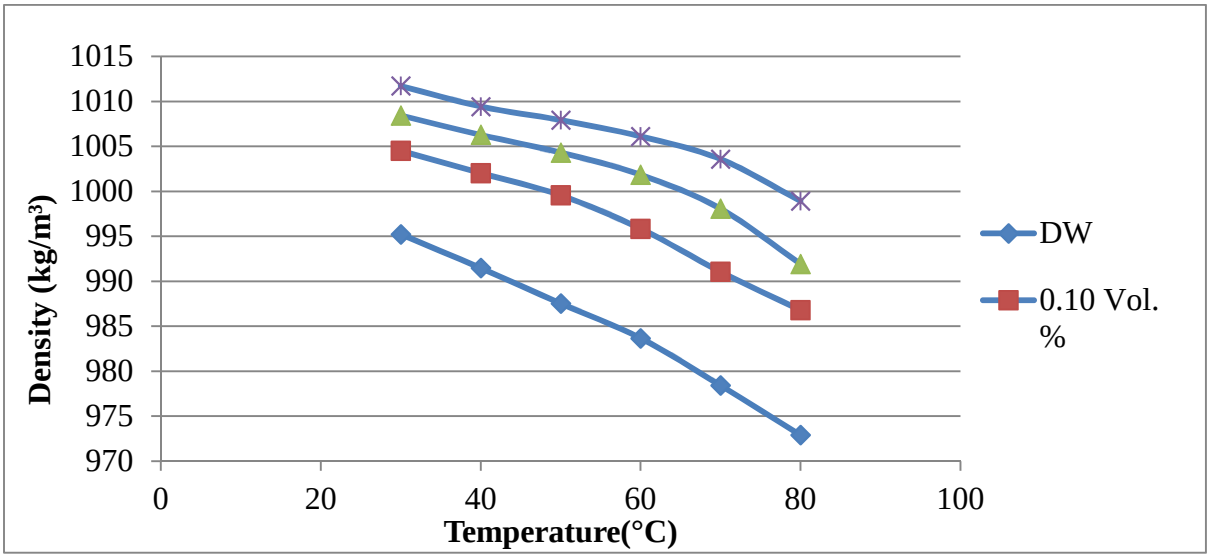

Fig. 5.1: Temperature-density graph

5.3 Viscosity measurement

Viscosity has measured by Brookfield LVDV-III rheometer for different concentrations (0.1 Vol. %, 0.25 Vol. % and 0.5 Vol. %) of CuO-distilled water based nanofluids for temperature range between 20ºC and 80ºC as shown in table 5.3. The variation of viscosity with temperature and concentrations are shown by Fig. 5.2. Viscosity of nanofluid increases as the concentration increases at same temperature but it decreases as temperature increases at same concentration.

Table 5.3: Viscosities of distilled water and CuO-distilled water based nanofluids

S. No	Temperature (°C)	Brookfield LVDV-III Rheometer (centi-Poise)			
		DW	0.1 Vol. % CuO	0.25 Vol. % CuO	0.5 Vol. % CuO
1	20	0.914	1.01	1.24	1.51
2	30	0.743	0.84	1.03	1.24
3	40	0.581	0.66	0.83	1.04
4	50	0.498	0.55	0.69	0.87
5	60	0.382	0.44	0.55	0.70
6	70	0.318	0.398	0.48	0.57
7	80	0.295	0.35	0.428	0.498

It can be seen from the Fig 5.2, that at 20°C, with the increase in the concentration of nanoparticles from 0.1 Vol. % to 0.5 Vol. %, viscosity of copper oxide-distilled water based nanofluids increases from 10.50 % to 65.21 % (i.e. 10.50 % for 0.1 Vol. % concentration, 35.67 % for 0.25 Vol. % concentration, 65.21 % for 0.50 Vol. % concentration) compared to base fluid i.e. distilled water.

And with the increase in temperature, viscosity of copper oxide-distilled water based nanofluids decreases. From 20°C to 80°C, viscosity decreases by 67.72 % for distilled water, 65.34 % for 0.1 Vol. % concentrations, 65.48 % for 0.25 Vol. % concentration and 67 % for 0.50 Vol. % concentrations.

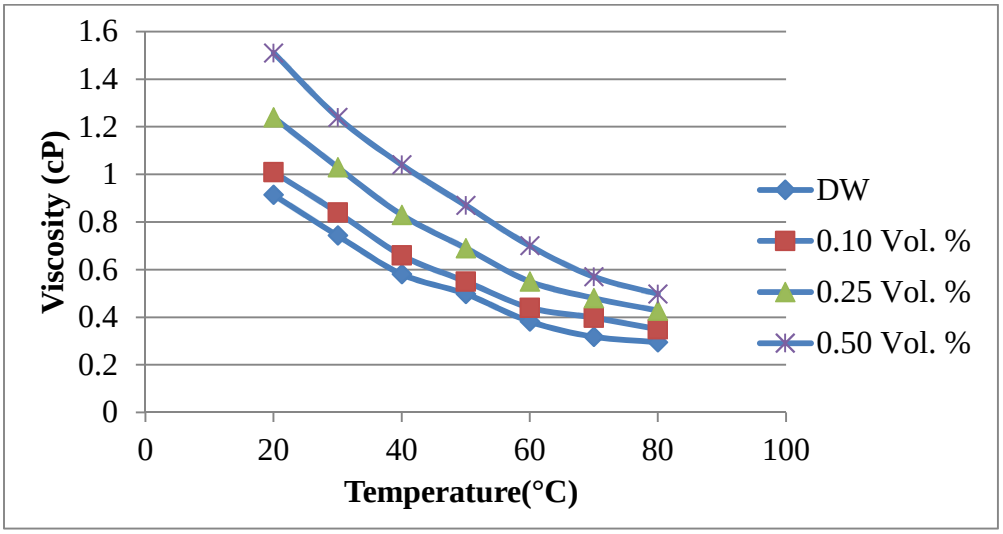

Fig. 5.2: Temperature-viscosity graph

5.4 Thermal conductivity measurement

Thermal conductivity of the samples has been measured by KD2 PRO thermal property analyzer from temperature range 20ºC to 80ºC. Different readings for distilled water and CuO-distilled water based nanofluids are shown in Table 5.4. The variation of thermal conductivity with temperature and concentration are shown by Fig. 5.3.

Table 5.4: Thermal conductivity of distilled water and CuO-distilled water based nanofluids

S. No.	Temperature (°C)	KD2 PRO reading Thermal conductivity (W/m.K)			
		DW	0.1 Vol. % CuO	0.25 Vol. % CuO	0.5 Vol. % CuO
1	20	0.590	0.594	0.598	0.602
2	30	0.600	0.610	0.617	0.620
3	40	0.610	0.622	0.636	0.641
4	50	0.620	0.646	0.658	0.660
5	60	0.630	0.665	0.672	0.685
6	70	0.640	0.681	0.701	0.710
7	80	0.650	0.694	0.724	0.733

It can be seen from the Fig 5.3, that at 20°C, with the increase in the concentration of nanoparticles from 0.1 Vol. % to 0.5 Vol. %, thermal conductivity of copper oxide-distilled water based nanofluids increases from 0.68 % to 2.0 % (i.e. 0.68 % for 0.1 Vol. % concentration, 1.36 % for 0.25 Vol. % concentration, 2.0 % for 0.50 Vol. % concentration) compared to base fluid i.e. distilled water.

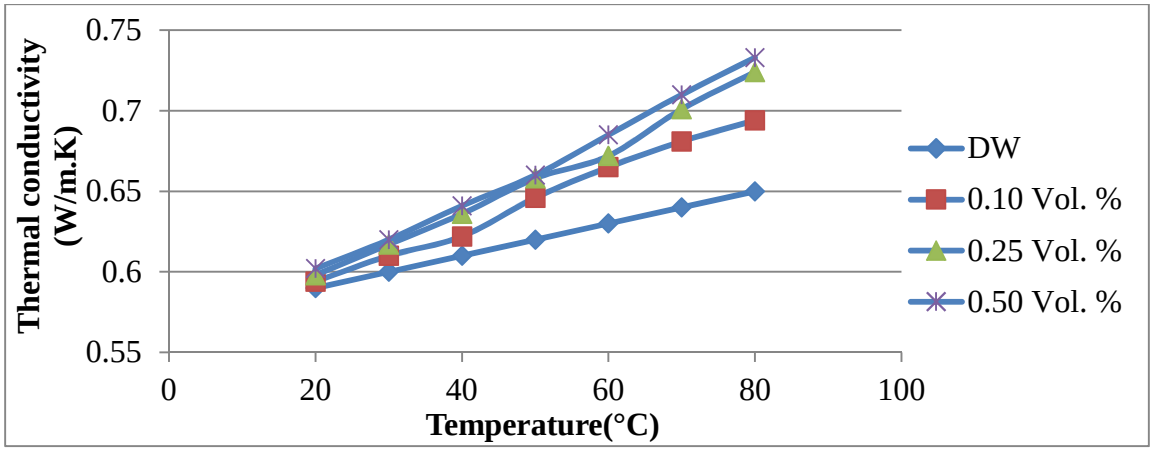

Fig. 5.3: Temperature-thermal conductivity graph

And with the increase in temperature, thermal conductivity of copper oxide-distilled water based nanofluids increases. From 20°C to 80 °C, thermal conductivity increases by 10.57 % for distilled water, 16.84 % for 0.1 Vol. % concentrations, 21.07 % for 0.25 Vol. % concentrations, and 21.76 % for 0.50 Vol. % concentrations.

5.5 Specific heat calculation

Specific heat for nanofluids has been calculated by using energy balance equation:

$$C_{nf} = \frac{\left(¤C_p + (1+¤)°_{bf} C_{bf}\right)}{°_{nf}} \tag{5.1}$$

Where,

C_{nf} = specific heat of the nanofluids

C_{bf} = specific heat of the base fluid

Φ = volume fraction

ρ_{bf} = density of the base fluid

ρ_{nf} = density of the nanofluids

Various readings of the distilled water and CuO-distilled water based nanofluids for various concentration has been calculated which are shown in Table 5.5:

Table 5.5: Specific heat of the distilled water and CuO-distilled water based nanofluids.

S. No.	Temperature (°C)	Specific heat (J/(kg.K))			
		DW	0.1 Vol. % CuO	0.25 Vol. % CuO	0.5 Vol. % CuO
1	30	4178.4	4139.07	4137.98	4136.16
2	40	4178.6	4133.85	4132.78	4130.99
3	50	4181.2	4129.19	4129.12	4127.37
4	60	4185.2	4133.36	4132.32	4130.59
5	70	4189.8	4135.09	4134.67	4132.98
6	80	4197.4	4137.74	4136.74	4135.08

The variation of the specific heat with the concentration is shown in Fig. 5.4. Specific heat decreases as the concentration of nanoparticles increases for example it can be seen from the graph that at 30°C, the specific heat of 0.1 Vol. %, 0.25 Vol. % and 0.50 Vol. % of copper oxide-distilled water based nanofluids decreases by 0.94 %, 0.97 % and 1.01 %, respectively compared to base fluid i.e. distilled water. But with temperature it decreases first and then increases after reaching the minimum value.

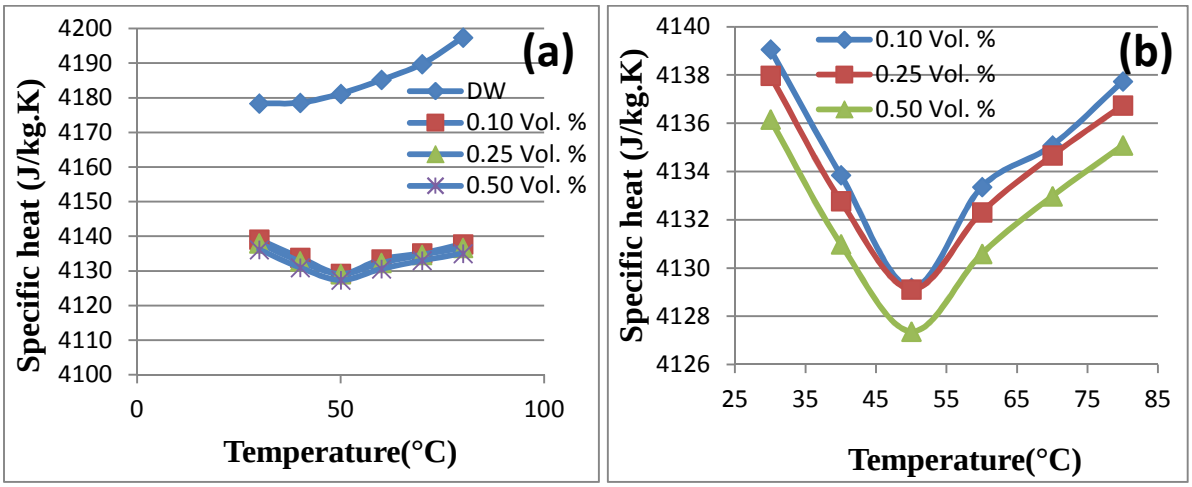

Fig. 5.4: Temperature-specific heat graph (a) shows DW, 0.10 Vol. %, 0.25 Vol. % and 0.50 Vol. % concentrations (b) shows 0.10 Vol. %, 0.25 Vol. % and 0.50 Vol. % concentrations.

5.6 Experimentation

Experimental setup is used for measuring the surface temperature of test section and the nanofluid flowing through the test section at different flow rates at constant heat flux.

5.6.1 Validation of experimental setup

Before conducting the experiment on nanofluid in test section the reliability and accuracy of experimental setup has been tested by using distilled water as the working fluid at constant heat flux flowing through test section at different flow rates. The results were compared with the result obtained from the Shah equation for laminar flow under constant heat flux.

Shah equation:

$$Nu = 1.953(\mathrm{Re}.\mathrm{Pr}.\frac{D}{x})^{1/3} \qquad (\mathrm{Re}.\mathrm{Pr}.\frac{D}{x}) \geq 33.3 \qquad (5.2)$$

$$Nu = 4.364 + 0.0722\,\mathrm{Re}\,\mathrm{Pr}\frac{D}{x} \qquad (\mathrm{Re}.\mathrm{Pr}.\frac{D}{x}) < 33.3 \qquad (5.3)$$

Various readings and calculated values of distilled water from experimental setup are shown in spread sheet Table 5.6.

Table 5.6: Various readings and calculated values of distilled water

Fluid	**Distilled Water**			
Flow Rate, LPH	10	20	25	30
Mass flow rate (kg/s)	0.00274	0.00549	0.00687	0.00826
Temperature (°C), T_1 Inlet	42.1	40.9	37.1	35.5
T_2	57.3	54.2	51.3	49.5
T_3	64.3	59.0	56.1	54.2
T_4	70.5	63.7	60.1	58.5
T_5	75.4	68.3	65.3	62.4
T_6	78.4	70.6	67.8	64.9
T_7	86.3	77.0	73.6	70.1
T_8 outlet	71.2	58.9	53.7	50.0
Average Surface Temperature	72.03	65.47	62.37	59.90
Fluid mean Temperature	56.65	49.90	45.40	42.75
Density (kg/m³)	984.20	986.35	989.74	990.79
Specific heat (J/(kg.K))	4184.00	4181.16	4179.68	4179.16
Viscosity (N.s/m²)	489 x 10^{-6}	549 x 10^{-6}	594 x 10^{-6}	623 x 10^{-6}
Conductivity (W/(m.K))	.650	.643	.638	.635
Prandtl Number	3.15	3.57	3.89	4.10
$T_{out} - T_{in}$	29.1	18.0	16.6	14.5
$\Delta T_{avg} = (T_s - T_m)$	15.38	15.57	16.97	17.15
Heat Flow rate, W	333.13	413.18	476.57	500.33
Heat Flux (W/m²)	7441.28	9229.5	10645.4	11176
Surface Area (m²)	.04477	.04477	.04477	.04477
Heat Transfer Coefficient (W/(m²K))	483.83	592.77	627.36	651.66
Reynolds number	750.9	1340.3	1550.1	1776.9
Nusselt Number	7.07	8.76	9.34	9.75

From shah equation Nusselt number is calculated and was compared with experimental data for distilled water at Reynolds number 750.9 and 1340.3.Table 5.7 shows the calculated shah and experimental local Nusselt number.

Table 5.7: Calculated experimental and shah local Nusselt number along the axial distance

S.NO.	alcu a x/D	Reynolds number Re = 750.9		Reynolds number Re = 1340.3	
		Local Nu Shah equation	Local Nu Experimental	Local Nu Shah equation	Local Nu Experimental
1	22.526	9.214	9.83	11.653	12.71
2	45.053	7.313	7.81	9.249	10.51
3	67.579	6.388	6.81	8.079	9.03
4	90.105	6.259	6.50	7.341	7.96
5	102.11	6.037	6.21	7.041	7.55
6	135.16	5.627	5.63	6.413	6.60

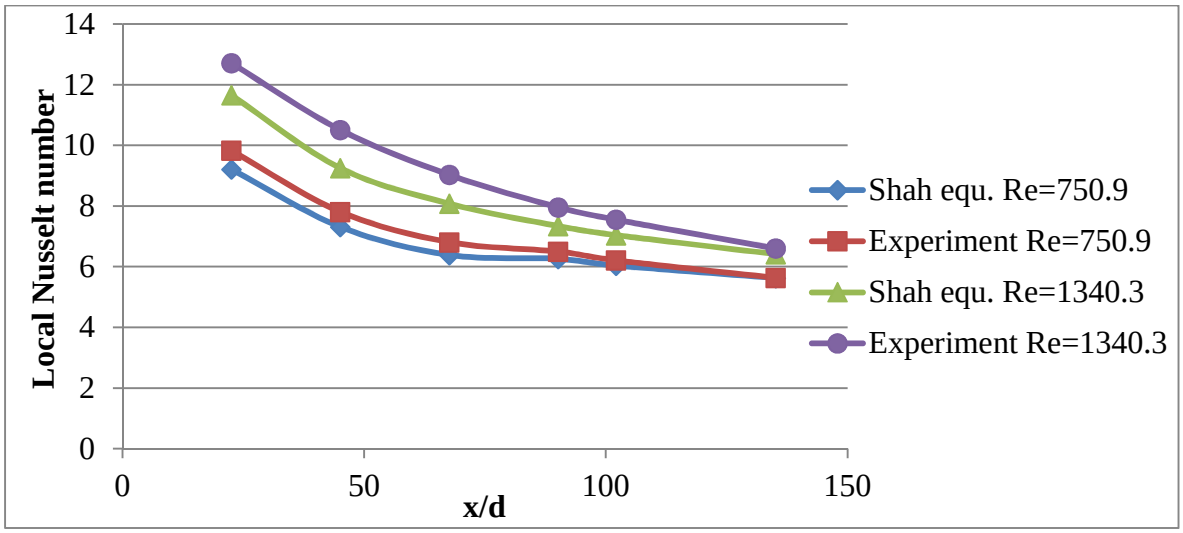

Fig. 5.5: Comparison between the experimental local Nusselt number and shah equations local Nusselt number versus axial distance

Fig. 5.5 shows the comparison between the Shah equation and the measurements using distilled water at Re = 750.9 and 1340.3 and the relative error are 4.48 % & 8.84 %, respectively. Hence good conformity can be seen between the results predicted by shah equation and those by the experiments.

5.6.2 Calculation of Reynolds number heat transfer coefficient and Nusselt number

The experiments were performed on constant power input at different flow rate i.e. 10 LPH, 20 LPH, 25 LPH and 30 LPH with distilled water and three different concentrations (0.1 Vol. %, 0.25 Vol. % and 0.5 Vol. %) of copper oxide with distilled water as base fluids. The voltage was 214.46 V and current was 1.709 A. Table 5.8 shows the various surface temperatures along the length of the test section and fluid inlet and outlet temperatures for different flow rate and different concentration of the nanofluids.

Table 5.8: Surface temperature of the test section and fluid inlet and outlet temperature at different flow rates and at various concentrations

Volume fraction (Φ) (%)	**Flow rate (LPH)**	**Inlet fluid (°C)**	**Surface temperature Outer side (°C)**						**Outlet Fluid (°C)**	**Average surface temperature (°C)**
		T_1	**T_2**	**T_3**	**T_4**	**T_5**	**T_6**	**T_7**	**T_8**	**$T_{s,o}$**
0.1	10	40.1	49.7	55.3	62.5	71.8	77.2	81.4	69.9	70.42
	20	39.1	42.1	47.8	54.4	59.7	63.3	71.2	56.6	61.13
	25	36.4	41.6	46.2	53.2	56.3	61.7	67.1	51.3	57.73
	30	34.9	40.3	45.6	50.3	55.2	59.5	63.6	48.6	55.63
0.25	10	38.5	46.8	54.3	61.9	68.4	76.2	80.5	68.8	69.02
	20	36.3	41.6	45.2	49.7	53.1	58.9	68.6	55.3	58.03
	25	35.7	40.3	45.6	50.1	54.9	59.3	67.1	53.1	57.34
	30	35.2	39.7	44.4	48.9	54.7	58.8	66.4	52.0	56.95
0.50	10	35.2	42.4	50.3	58.1	66.3	71.5	79.6	66.6	66.73
	20	34.7	40.1	44.9	50.2	55.1	59.2	65.3	54.4	56.34
	25	33.2	37.9	42.7	47.3	52.8	57.1	63.9	51.8	54.54
	30	32.8	37.1	41.3	45.6	50.9	54.3	62.3	50.9	52.95

From the above fluid inlet and outlet temperature for particular flow rate and concentration fluid mean temperature was calculated. At the calculated fluid mean temperature the various thermo-physical properties of the fluid were measured. With the help of formulae already mention in the previous chapter and using the values of these properties, the values of Reynolds number and heat transfer coefficient, Nusselt number are calculated. Table 5.9, Table 5.10 and Table 5.11

shows the calculated value of the Reynolds number, heat transfer coefficient and Nusselt number.

Table 5.9: Calculated value of the Reynolds number at various flow rates

S.NO.	Flow rate (LPH)	Reynolds number			
		DW	0.1 Vol. % CuO	0.25 Vol. % CuO	0.5 Vol. % CuO
1	10	750.9	741.88	585.18	438.4
2	20	1340.3	1298.22	999.48	779.38
3	25	1550.1	1507.24	1218.09	940.06
4	30	1776.9	1748.88	1441.76	1117.09

Table 5.10: Calculated value of the heat transfer coefficient at various flow rates

S.NO.	Flow rate (LPH)	Heat transfer coefficient (W/m^2K)			
		DW	0.1 Vol. % CuO	0.25 Vol. % CuO	0.5 Vol. % CuO
1	10	483.83	494.65	508.11	513.06
2	20	592.77	677.69	782.58	866.03
3	25	627.36	690.12	875.59	1000.98
4	30	651.66	766.43	976.88	1270.96

Table 5.11: Calculated value of the Nusselt number at various flow rates

S.NO.	Flow rate (LPH)	Nusselt number			
		DW	0.1 Vol. % CuO	0.25 Vol. % CuO	0.5 Vol. % CuO
1	10	7.07	7.174	7.280	7.36
2	20	8.76	10.04	11.46	12.67
3	25	9.34	10.39	12.88	14.72
4	30	9.75	11.63	14.41	18.72

Table 5.9 shows the calculated value of the Reynolds number at different flow rate and at different concentration. From graph it is observed that the Reynolds number is increases with the flow rate. The reason is that it is directly proportional to the velocity and velocity always increases with increasing the flow rate.

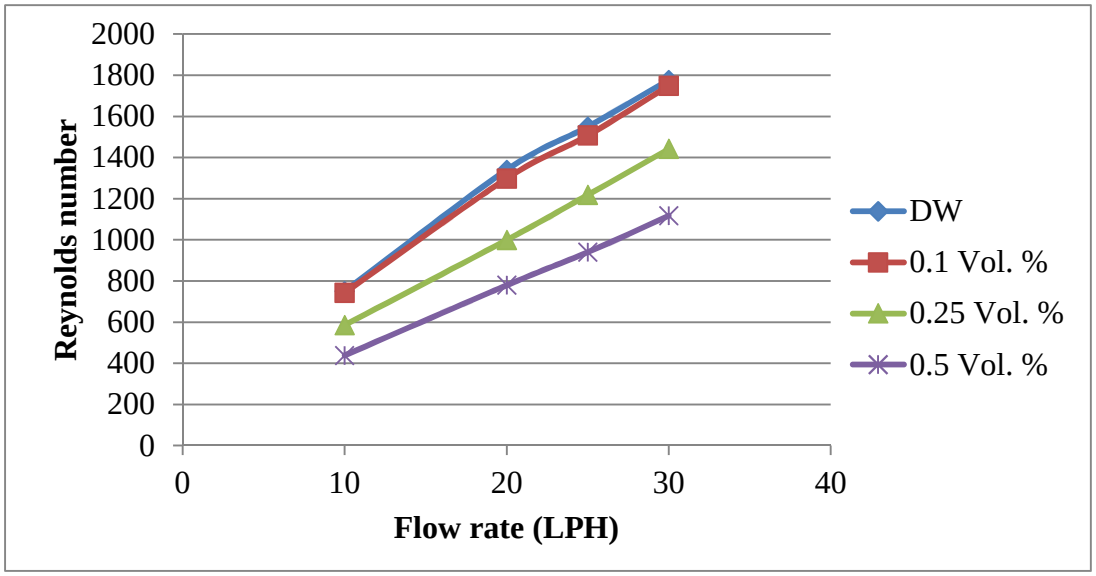

Fig 5.6: Flow rate versus Reynolds number at various volume concentrations

But it is not true for the concentration as shown by the Fig. 5.6. It decreases with the increase in concentration. The reason is that it is inversely proportion to the viscosity and viscosity increases with the increase in concentration. But increase in concentration also increases the density which is directly proportional the Reynolds number. So, both density and viscosity increases with the increase in concentration. But the effect of viscosity is predominated or more than density hence Reynolds number decreases.

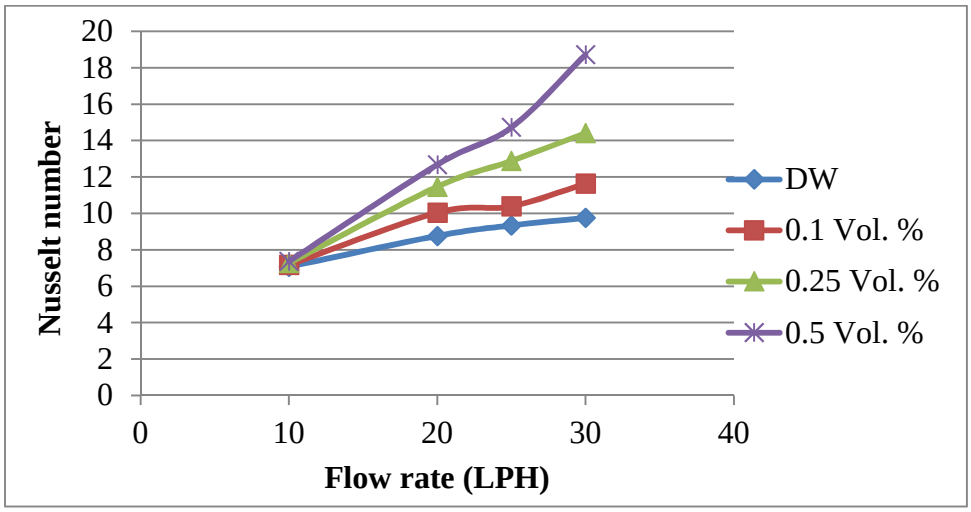

Fig. 5.7: Flow rate versus Nusselt number at various volume concentrations

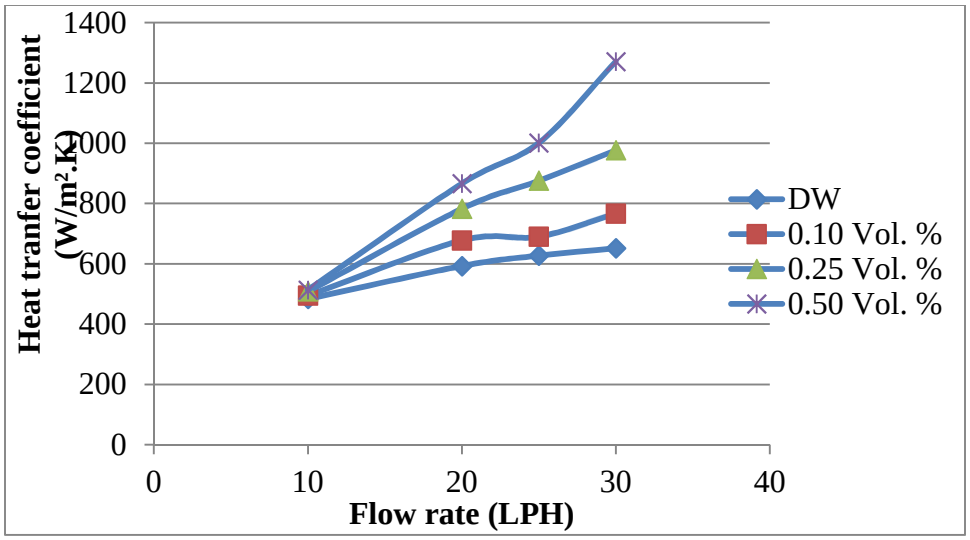

Fig. 5.8: Flow rate versus heat transfer coefficient at various volume concentrations

Fig. 5.8 shows the variation of the average heat transfer coefficient with different flow rate at given concentration. The value of average heat transfer coefficient increases with increase in flow rate and also with the increase in the concentration. Here heat transfer coefficient means the average heat transfer coefficient.

At 10 LPH flows rate of nanofluid, there is an increment of 2.23 % in heat transfer coefficient at 0.1 Vol. % concentration of CuO-distilled water based nanofluid, 5.0 % increment in heat transfer coefficient at 0.25 Vol. % of CuO-distilled water based nanofluid and 6.04 % increment in heat transfer coefficient at 0.5 Vol. % of CuO-distilled water based nanofluid as compared to distilled water heat transfer coefficient.

At 20 LPH flows rate of nanofluid, there is an increment of 14.33 % in heat transfer coefficient at 0.1 Vol. % concentration of CuO-distilled water based nanofluid, 32.0 % increment in heat transfer coefficient at 0.25 Vol. % of CuO-distilled water based nanofluid and 46.1 % increment in heat transfer coefficient at 0.5 Vol. % of CuO-distilled water based nanofluid as compared to distilled water heat transfer coefficient.

At 25 LPH flows rate of nanofluid, there is an increment of 10.0 % in heat transfer coefficient at 0.1 Vol. % concentration of CuO-distilled water based nanofluid, 39.57 % increment in heat transfer coefficient at 0.25 Vol. % of CuO-distilled water based nanofluid and 59.55 %

increment in heat transfer coefficient at 0.5 Vol. % of CuO-distilled water based nanofluid as compared to distilled water heat transfer coefficient.

At 30 LPH flows rate of nanofluid, there is an increment of 17.61 % in heat transfer coefficient at 0.1 Vol. % concentration of CuO-distilled water based nanofluid, 49.90 % increment in heat transfer coefficient at 0.25 Vol. % of CuO-distilled water based nanofluid and 95.03 % increment in heat transfer coefficient at 0.5 Vol. % of CuO-distilled water based nanofluid as compared to distilled water heat transfer coefficient.

Table 5.12: Reynolds number and Nusselt number at various concentrations

S.NO.	DW		0.1 Vol. % CuO		0.25 Vol. % CuO		0.5 Vol. % CuO	
	Re	Nu	Re	Nu	Re	Nu	Re	Nu
1	750.9	7.07	741.88	7.174	585.18	7.28	438.4	7.36
2	1340.3	8.76	1298.22	10.04	999.479	11.46	779.38	12.67
3	1550.1	9.34	1507.24	10.39	1218.09	12.88	940.06	14.72
4	1776.9	9.75	1748.88	11.63	1441.76	14.41	1117.1	18.72

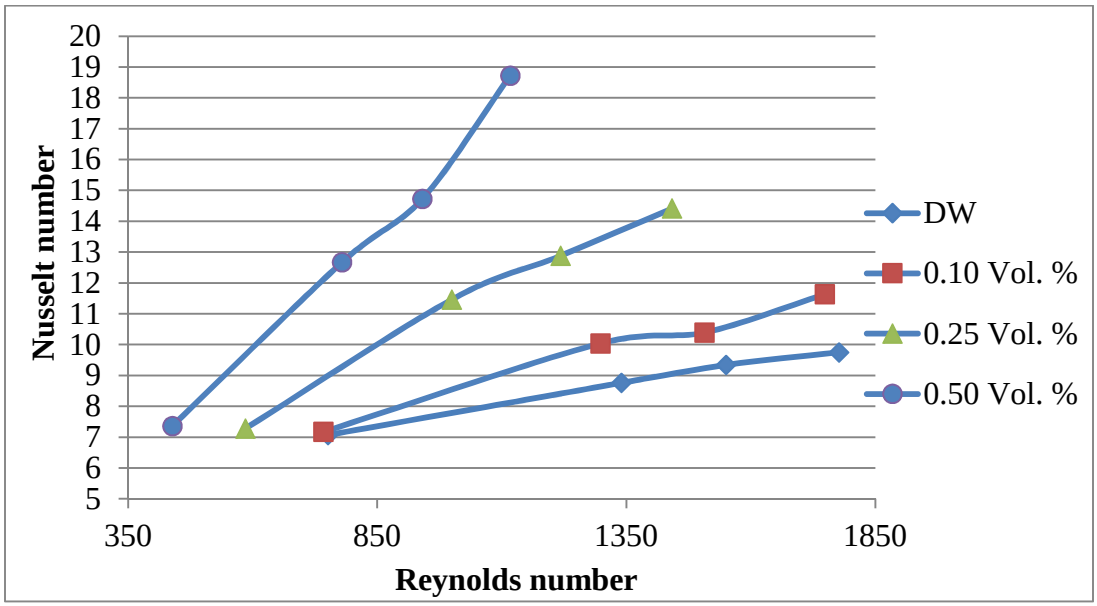

Fig. 5.9: Reynolds number versus Nusselt number at various volume concentrations

The variation of Nusselt number with Reynolds number is shown by Fig. 5.9 and the generalized power equation of Nusselt number with Reynolds number for distilled water and copper oxide-distilled water based nanofluids is given by equation 5.4 to equation 5.7.

$$Nu = 0.0199Re^{0.9709} \quad \text{for DW} \quad (5.4)$$

$$Nu = 0.0571Re^{0.7629} \quad \text{for 0.1 Vol. \%} \quad (5.5)$$

$$Nu = 0.1868Re^{0.5526} \quad \text{for 0.25 Vol. \%} \quad (5.6)$$

$$Nu = 0.5848Re^{0.3764} \quad \text{for 0.5 Vol. \%} \quad (5.7)$$

5.6.3 Pressure drop measurement

The pressure is measured by the u-tube differential manometer for different flow rate (10 LPH, 20 LPH, 25 LPH and 30 LPH) and readings are shown in table 5.13.

Table 5.13: Values of pressure drop at different flow rates and concentrations

S.NO.	Flow rate (LPH)	Pressure drop (Pa)			
		DW	0.1 Vol. % CuO	0.25 Vol. % CuO	0.5 Vol. % CuO
1	10	11.58	14.68	19.68	21.75
2	20	24.19	27.47	31.55	34.64
3	25	33.98	37.32	41.42	47.51
4	30	41.63	44.22	49.32	54.45

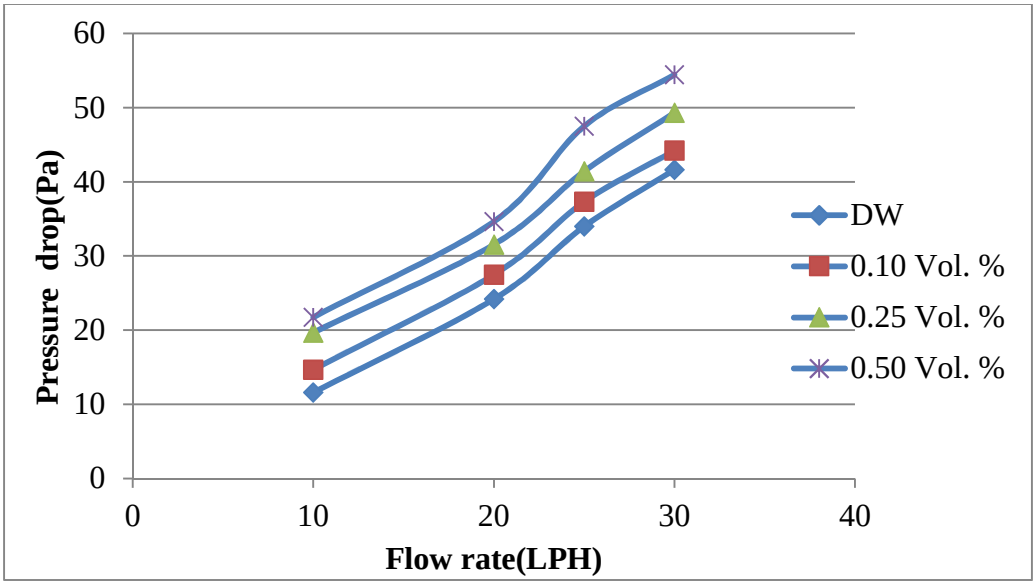

Fig. 5.10: Flow rate versus pressure drop at various volume concentrations

Fig. 5.10 shows the variation of the pressure drop with the flow rate and concentration. The value pressure drop increases with the increase in flow rate. The pressure drop increases with nanoparticles concentration. The pressure drops are high at higher volume fractions. For example at 30 LPH flow rate for 0.5 Vol. % is 30.7 % higher than distilled water and for the same flow rate but at 0.1 Vol. % it is 6.2 % higher than the distilled water. So using the nanofluids at higher concentration is also not good as it may create penalty in pressure drop.

Table 5.14 show the variation of the friction factor with the Reynolds number. It decreases with the increase in Reynolds number but increases with the increase in concentration. It is because of the decrease in Reynolds number with the increase in concentration as shown in Fig. 5.11.

Table 5.14: Values of friction factors and Reynolds number at various concentrations

S.NO.	DW		0.1 Vol. % CuO		0.25 Vol. % CuO		0.5 Vol. % CuO	
	Re	f	Re	f	Re	f	Re	f
1	750.9	0.09704	741.88	0.12135	585.18	0.16176	438.4	0.17799
2	1340.3	0.05057	1298.22	0.05663	999.479	0.06472	779.38	0.07489
3	1550.1	0.04531	1507.24	0.042	1218.09	0.05437	940.06	0.06214
4	1776.9	0.0385	1748.88	0.04046	1441.76	0.04495	1117.1	0.04944

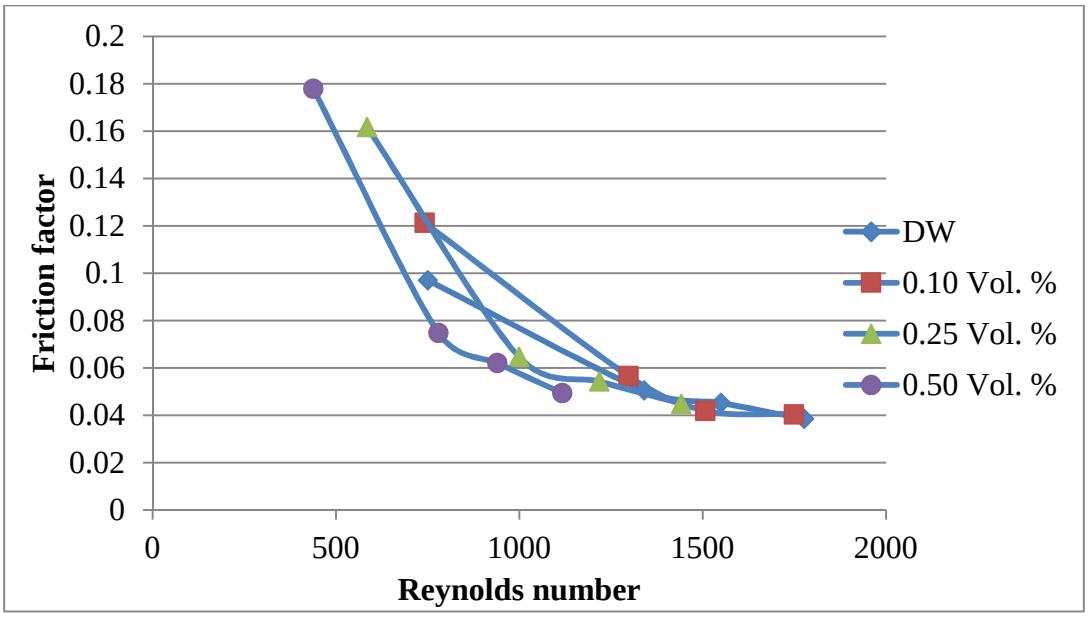

Fig. 5.11: Reynolds number versus friction factor at various volume concentrations

The generalized power equation of friction factor with Reynolds number for distilled water and copper oxide-distilled water based nanofluids is given by equation 5.8 to equation 5.11.

$f = 114.38Re^{-1.069}$ for DW (5.8)

$f = 887.73Re^{-1.348}$ for 0.1 Vol. % (5.9)

$f = 1480.7Re^{-1.438}$ for 0.1 Vol. % (5.10)

$f = 743.03Re^{-1.374}$ for 0.1 Vol. % (5.11)

Table 5.15: Values of friction factors at various and concentrations

S.NO.	Flow rate (LPH)	Friction factor			
		DW	0.1 Vol. % CuO	0.25 Vol. % CuO	0.5 Vol. % CuO
1	10	0.09704	0.12135	0.16176	0.17799
2	20	0.05057	0.05663	0.06472	0.07489
3	25	0.04531	0.042	0.05437	0.06214
4	30	0.0385	0.04046	0.04495	0.04944

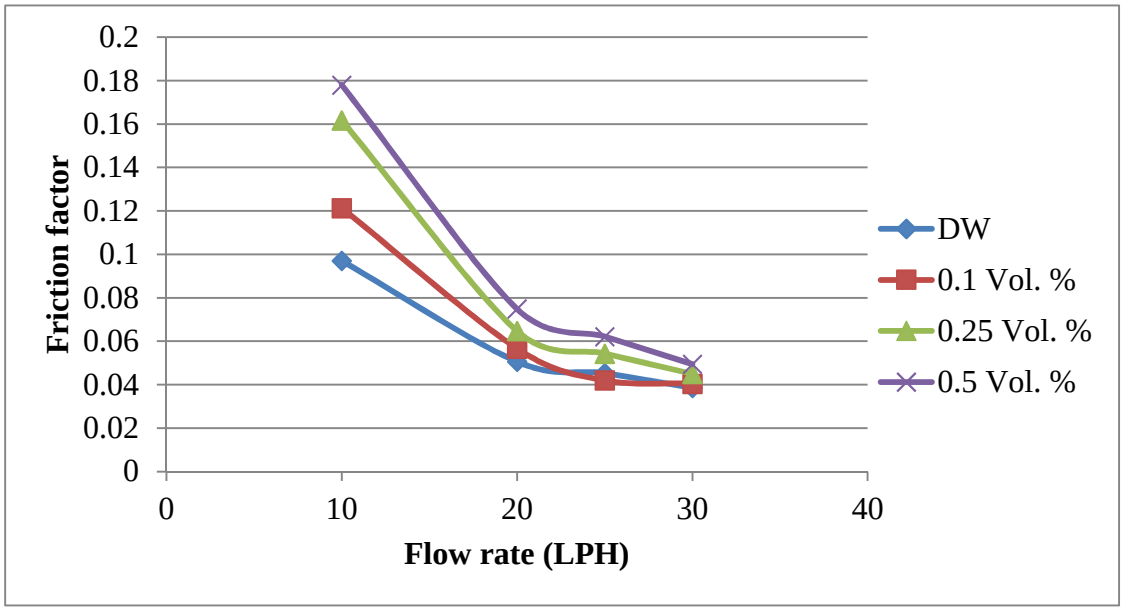

Fig. 5.12: Variation of the friction factor with flow rate and concentration

Fig. 5.12 shows the variation of the friction factor with the flow rate at different concentration. Friction factor decreases continuously with the increase in flow rate. For nanofluids it increases with the increase in concentration except for 0.1 Vol. % at 25 LPH flow rate where it shows the decrement of 7.3 %, when compared with distilled water for the same flow rate.

Conclusion

In this chapter the results of the thermo-physical properties (density, viscosity, thermal conductivity and specific heat) are discussed. All the results of the properties are measured at different temperature and concentrations. These results are used when heat transfer coefficient and pressure drop are calculated at different mean temperature. The variation of both heat transfer and pressure drop with Reynolds number and concentrations are discussed.

Conclusions

The purpose of this study was to observe and measure the heat transfer and pressure drop characteristics of the distilled water and the copper oxide-distilled water based nanofluid flowing in a horizontal circular tube in a laminar flow under constant heat flux condition. The CuO-distilled water based nanofluids are prepared by dispersing the nanoparticles of 40nm size into distilled water and using sodium dodecyl sulphate as surfactant and the prepared nanofluids are sonicated with the help of ultra sonicator water bath. The nanofluids are made in three different concentrations i.e. 0.1 Vol. %, 0.25 Vol. % and 0.5 Vol. %. The thermo-physical properties needed to calculate the heat transfer coefficient and pressure drop are measured as follow: the density is measured by pycnometer (specific gravity bottle), viscosity is measured by Brookfield LVDV-III Rheometer and thermal conductivity is measured by KD2 pro thermal property analyzer. Based on experimental results the following discussions are drawn:

- The addition of the nanoparticles in the base fluid increases the density. At 30°C, the density of copper oxide-distilled water based nanofluids increases from 0.93 % to 1.66 % with the increase in the concentration of nanoparticles from 0.1 Vol. % to 0.50 Vol. %. It decreases continuously with the increase in temperature.
- The viscosity increases with the increase in concentration. At 30°C, the viscosity of copper oxide-distilled water based nanofluids increases from 10.50 % to 65.21 % with the increase in the concentration of nanoparticles from 0.1 Vol. % to 0.50 Vol. %. It decreases continuously with the increase in temperature.
- The thermal conductivity is also increases with the addition of the nanoparticles. At 30°C, the viscosity of copper oxide-distilled water based nanofluids increases from 0.68 % to 2.0 % with the increase in the concentration of nanoparticles from 0.1 Vol. % to 0.50 Vol. %. It increases continuously with the increase in temperature.
- The specific heat was first decreases and then increases with temperature. But with the increase in concentration it decreases.
- The experimental local Nusselt number of distilled water is compared with Nusselt number obtained by the well known shah equation for laminar flow under constant heat flux condition for validation of the experimental set up. The relative errors are 4.48 % and 8.84 % for the Reynolds number 750.9 and 1340.3, respectively.

- Reynolds number increases with temperature but decreases with the increase in concentrations.
- Heat transfer coefficient increases with increase in both flow rate and concentration. for example At 20 LPH flows rate of nanofluid, there is an increment of 14.33 % in heat transfer coefficient at 0.1 Vol. % of CuO-distilled water based nanofluid, 32.0 % increment in heat transfer coefficient at 0.25 Vol. % of CuO-distilled water based nanofluid and 46.1 % increment in heat transfer coefficient at 0.5 Vol. % of CuO-distilled water based nanofluid as compared to distilled water heat transfer coefficient.
- And with the increase in flow rate, heat transfer coefficient of copper oxide-distilled water based nanofluids increases. From 10 LPH to 30 LPH, heat transfer coefficient increases by 34.69 % for distilled water, 54.94 % for 0.1 Vol. % concentration, 92.28 % for 0.25 Vol. % concentration and 147.72 % for 0.50 Vol. % concentrations.
- Nusselt number increases with increase in both Reynolds number and concentrations.
- Pressure drop increases with increase in flow rate and concentrations.
- Friction factor decreases with increase in Reynolds number but increases with the increase in concentration.
- Friction factor decreases with increase in flow rate. For 0.5 Vol. %, the decrement in friction factor of copper oxide-distilled water based nanofluids is 72.22 % with the increase in the flow rate from 10 LPH to 30 LPH.

Future scope of work

1. The nanofluids prepared for the experimentation are not long term stable. Since the stability of the nanofluids is matter of great concern. So there is a need of more work in the field of stability.

2. A little literature is available on the specific heat of the nanofluids. Since the specific heat is also required for the calculation of the heat transfer coefficient. So there should be requirement for more experimentation on the specific heat of the nanofluids.

3. The experiments with more concentration can be performed to evaluate the heat transfer and pressure drop characteristics.

4. An empirical model is needed to be required for the measurement of the heat transfer coefficient and friction factor.

.

Sample calculation

Mass of copper oxide (0.1 Vol. %)

For 50 ml of sample

$$Volume\ \ fraction\ ¤ = \frac{V_{nanoparticles}}{V_{total}} \times 100$$

$$Volume\ \ fraction\ ¤ = \frac{\frac{m_{CuO}}{°_{CuO}}}{V_{total}} \times 100$$

$$m_{CuO} = \frac{¤ \times V_{total} \times °_{CuO}}{100}$$

Given,

$$°_{CuO} = 6.4\ gm/cm^3$$

$$V_{total} = 50\ ml$$

$$¤ = .1$$

$$m_{CuO} = \frac{0.1 \times 50 \times 6.4}{100} = .32\ gm$$

Calculation of heat transfer coefficient for 0.1 Vol. % concentration at 30 LPH

Table: Outer surface temperature, fluid inlet and outlet temperature

Volume fraction Φ (%)	Flow rate LPH	Inlet fluid (°C)	Surface temperature Outer side (°C)						Outlet Fluid (°C)	Average surface temperature (°C)	Pressure drop (mm)
		T_1	T_2	T_3	T_4	T_5	T_6	T_7	T_8	$T_{s,o}$	h
0.1	10	40.1	49.7	55.3	62.5	71.8	77.2	81.4	69.9	70.42	4.5

Now calculating the mean temperature

$$T_{bm} = \frac{(T_1 + T_8)}{2} = \frac{(40.1 + 69.9)}{2} = 55°C$$

At this fluid mean temperature, thermo-physical properties of nanofluids are given below:

$k = 0.655\ W/m.K$

$C_p = 4131.275\ J/kg.K$

$« = 495 \times 10^{-6}\ N.s/m^2$

$$Discharge = 10\ LPH = 2.7778 \times 10^{-6}\ m/s$$

$$\overline{V} = \frac{Discharge}{A_c} = \frac{2.7778 \times 10^{-6}}{\frac{®}{4} \times D^2} = \frac{2.7778 \times 10^{-6}}{\frac{®}{4} \times .0095^2} = .03919\ m/s$$

$$\text{Re} = \frac{° \overline{V} D}{«} = 741.88$$

$$\dot{m} = \rho \times A_c \times \overline{V} = 997.70 \times 0.4477 \times 0.039190 = 0.00277\ kg/s$$

$$Q_1 = V \times I = 366.51\,W$$

$$Q_2 = m.C_p.(T_8 - T_1) = 0.00277 \times 4131.275 \times (69.9 - 40.1) = 340.07\,W$$

$$q = \frac{Q_2}{A_s} = \frac{340.07}{\pi \times 0.0095 \times 1.5} = 7617.55\,W/m^2$$

$$Q_2 = 2\pi kl \frac{(T_{so} - T_{si})}{\ln \frac{r_o}{r_i}}$$

$$340.07 = 2 \times \pi \times 401 \times 1.5 \frac{(70.4 - T_{si})}{\ln \frac{0.00635}{0.00475}}$$

$$T_{si} = 70.4°C$$

$$h = \frac{q}{(T_{si} - T_{bm})} = \frac{7617.55}{(70.42 - 55)} = 494.646\,W/m^2.K$$

$$Nu = \frac{h \bullet k}{D} = 7.174$$

Calculation of pressure drop and friction factor of the nanofluids

Reading measured by u-tube differential manometer (ΔH) is 1.5 mm. at 0.1 Vol. % and 10 LPH flow rate.

Pressure drop

$$\Delta p = \Delta H \rho g = 0.0015 \times 997.70 \times 9.81 = 14.68\ Pa$$

Friction factor

$$f = \frac{\Delta p}{(\frac{1}{2} \rho \overline{V^2})} (\frac{D}{L}) = \frac{14.68}{(\frac{1}{2} \times 997.70 \times .03919^2)} \times (\frac{0.0095}{1.5}) = 0.12135$$

Annexure-B

All the readings were taken at power voltage = 211.14V and current = 1.682A.

Table: showing reading of the steady state for 0.1 Vol. % for 10 LPH flow rate.

Time (minutes)	**Inlet fluid (°C)**	**Surface temperature Outer side (°C)**						**Outlet Fluid (°C)**	**Pressure drop (mm)**
	T_1	**T_2**	**T_3**	**T_4**	**T_5**	**T_6**	**T_7**	**T_8**	**h**
15	32.8	34.3	35.1	36.7	38.2	39.3	39.9	37.7	1.5
30	35.7	40.3	44.6	49.9	55.3	60.1	55.7	40.7	1.5
45	36.8	44.9	48.3	53.4	57.8	62.1	67.2	45.3	1.5
60	38.3	46.8	51.8	56.5	60.8	65.3	72.9	50.1	1.5
75	39.8	49.7	54.9	59.8	65.6	69.1	75.7	57.6	1.5
90	40.1	49.6	55.3	62.5	71.8	77.2	81.3	69.9	1.5
120	40.1	49.6	55.3	62.5	71.8	77.2	81.3	69.9	1.5

Table: showing reading of the steady state for 0.1 Vol. % for 20 LPH flow rate.

Time (minutes)	**Inlet fluid (°C)**	**Surface temperature Outer side (°C)**						**Outlet Fluid (°C)**	**Pressure drop (mm)**
	T_1	**T_2**	**T_3**	**T_4**	**T_5**	**T_6**	**T_7**	**T_8**	**h**
15	32.7	34.2	35.3	36.4	38.4	39.1	40.1	38.2	2.8
30	35.9	38.2	41.9	43.1	47.5	53.4	54.4	41.7	2.8
45	36.1	40.8	44.5	52.3	57.3	57.7	68.8	44.6	2.8
60	37.5	41.6	46.2	53.9	58.8	59.6	69.4	52.7	2.8
75	38.3	41.9	47.1	54.1	59.3	62.9	70.8	54.5	2.8
90	39.1	42.1	47.8	54.4	59.7	63.3	71.2	56.6	2.8
120	39.1	42.1	47.8	54.4	59.7	63.3	71.2	56.6	2.8

Table: showing reading of the steady state for 0.1 Vol. % for 25 LPH flow rate.

Time (minutes)	Inlet fluid (°C)	Surface temperature Outer side (°C)						Outlet Fluid (°C)	Pressure drop (mm)
	T_1	T_2	T_3	T_4	T_5	T_6	T_7	T_8	h
15	32.5	33.5	35.6	36.3	37.6	38.7	39.5	37.4	3.8
30	34.8	36.2	41.9	39.7	39.7	49.8	53.1	38.6	3.8
45	35.6	38.7	43.5	43.8	46.3	54.5	63.9	42.3	3.8
60	35.9	40.1	45.7	48.9	52.9	57.1	66.4	46.9	3.8
75	36.2	41.1	46.3	51.8	54.2	60.5	66.9	49.7	3.8
90	36.4	41.6	46.2	53.2	56.3	61.7	67.1	51.3	3.8
120	36.4	41.6	46.2	53.2	56.3	61.7	67.1	51.3	3.8

Table: showing reading of the steady state for 0.1 Vol. % for 30 LPH flow rate.

Time (minutes)	Inlet fluid (°C)	Surface temperature Outer side (°C)						Outlet Fluid (°C)	Pressure drop (mm)
	T_1	T_2	T_3	T_4	T_5	T_6	T_7	T_8	h
15	32.7	33.6	35.5	36.8	37.3	38.5	39.6	37.6	4.5
30	33.7	36.6	38.6	40.7	42.5	46.7	47.1	43.1	4.5
45	34.1	37.1	42.7	43.5	48.9	53.9	55.7	45.7	4.5
60	34.5	38.2	43.1	47.1	53.1	55.3	60.9	46.2	4.5
75	34.8	39.3	44.5	49.2	54.2	57.8	62.5	47.7	4.5
90	34.9	40.3	45.6	50.3	55.2	59.5	63.6	48.6	4.5
120	34.9	40.3	45.6	50.3	55.2	59.5	63.6	48.6	4.5

Table: showing reading of the steady state for 0.25 Vol. % for 10 LPH flow rate.

Time (minutes)	Inlet fluid (°C)	Surface temperature Outer side (°C)						Outlet Fluid (°C)	Pressure drop (mm)
	T_1	T_2	T_3	T_4	T_5	T_6	T_7	T_8	h
15	32.4	33.8	35.5	36.4	37.8	38.5	39.5	37.6	2
30	33.6	36.9	43.6	47.7	49.5	52.7	55.1	48.1	2
45	34.8	39.4	47.7	50.5	56.9	64.9	68.7	59.7	2
60	35.7	43.9	50.1	57.1	64.1	69.3	76.9	65.2	2
75	37.8	45.7	53.8	60.2	67.5	75.8	78.9	67.7	2
90	38.5	46.8	54.3	61.9	68.4	76.2	80.5	68.8	2
120	38.5	46.8	54.3	61.9	68.4	76.2	80.5	68.8	2

Table: showing reading of the steady state for 0.25 Vol. % for 20 LPH flow rate.

Time (minutes)	Inlet fluid (°C)	Surface temperature Outer side (°C)						Outlet Fluid (°C)	Pressure drop (mm)
	T_1	T_2	T_3	T_4	T_5	T_6	T_7	T_8	h
15	32.8	33.4	35.7	36.9	37.6	38.6	39.8	37.3	3.2
30	33.5	35.6	39.6	41.7	43.5	47.7	51.1	43.6	3.2
45	34.2	36.1	41.7	44.5	45.9	53.9	60.7	45.4	3.2
60	34.3	37.2	44.1	47.1	49.1	55.7	64.9	46.8	3.2
75	35.7	39.5	45.5	48.2	52.2	57.8	67.5	47.9	3.2
90	36.3	41.6	45.2	49.7	53.1	58.9	68.6	55.3	3.2
105	36.3	41.6	45.2	49.7	53.1	58.9	68.6	55.3	3.2

Table: showing reading of the steady state for 0.25 Vol. % for 25 LPH flow rate

Time (minutes)	Inlet fluid (°C)	Surface temperature Outer side (°C)						Outlet Fluid (°C)	Pressure drop (mm)
	T_1	T_2	T_3	T_4	T_5	T_6	T_7	T_8	h
15	32.5	33.2	35.8	36.6	37.9	38.1	39.2	37.8	4.2
30	33.1	35.6	38.7	41.7	44.5	50.7	49.1	42.1	4.2
45	34.6	37.1	42.3	44.5	47.9	54.9	57.7	46.7	4.2
60	34.9	38.2	43.9	48.1	50.1	55.7	64.9	49.2	4.2
75	34.6	39.3	44.3	49.6	53.2	57.1	66.5	42.7	4.2
90	35.7	40.3	45.6	50.1	54.9	59.3	67.1	53.1	4.2
105	35.7	40.3	45.6	50.1	54.9	59.3	67.1	53.1	4.2

Table: showing reading of the steady state for 0.25 Vol. % for 30 LPH flow rate

Time (minutes)	Inlet fluid (°C)	Surface temperature Outer side (°C)						Outlet Fluid (°C)	Pressure drop (mm)
	T_1	T_2	T_3	T_4	T_5	T_6	T_7	T_8	h
15	32.3	33.7	35.1	36.6	37.9	38.2	39.8	37.2	5
30	32.9	36.3	37.6	41.7	46.5	47.7	50.1	45.1	5
45	33.5	37.6	41.7	42.5	50.9	52.9	57.7	48.7	5
60	34.7	38.1	42.1	45.1	52.1	53.3	64.9	49.2	5
75	34.9	39.2	43.5	47.2	53.2	56.8	65.5	49.7	5
90	35.2	39.7	44.4	48.9	54.7	58.8	66.4	52.0	5
105	35.2	39.7	44.4	48.9	54.7	58.8	66.4	52.0	5

Table: showing reading of the steady state for 0.5 Vol. % for 10 LPH flow rate

Time (minutes)	Inlet fluid (°C)	Surface temperature Outer side (°C)						Outlet Fluid (°C)	Pressure drop (mm)
	T_1	T_2	T_3	T_4	T_5	T_6	T_7	T_8	h
15	32.6	33.5	35.6	36.3	37.4	38.7	39.4	37.5	2.2
30	32.7	37.3	40.3	44.7	49.5	49.7	54.1	47.9	2.2
45	33.8	38.6	45.7	50.5	58.9	60.9	65.7	55.7	2.2
60	34.7	40.1	48.1	56.1	63.1	66.3	70.9	59.2	2.2
75	35.1	41.2	49.5	57.2	65.2	69.8	78.5	65.7	2.2
90	35.2	42.4	50.3	58.1	66.3	71.5	79.6	66.6	2.2
120	35.2	42.4	50.3	58.1	66.3	71.5	79.6	66.6	2.2

Table: showing reading of the steady state for 0.5 Vol. % for 20 LPH flow rate

Time (minutes)	Inlet fluid (°C)	Surface temperature Outer side (°C)						Outlet Fluid (°C)	Pressure drop (mm)
	T_1	T_2	T_3	T_4	T_5	T_6	T_7	T_8	h
15	32.5	33.1	35.8	36.4	37.7	38.6	39.3	37.7	3.5
30	33.4	36.4	38.8	44.7	47.5	49.7	49.4	47.1	3.5
45	33.9	37.2	41.4	46.5	53.9	53.9	57.1	49.7	3.5
60	34.3	37.9	43.5	47.1	53.1	56.3	62.9	50.2	3.5
75	34.9	39.5	44.4	49.2	54.3	58.8	64.1	53.7	3.5
90	34.7	40.1	44.9	50.2	55.1	59.2	65.3	54.4	3.5
105	34.7	40.1	44.9	50.2	55.1	59.2	65.3	54.4	3.5

Table: showing reading of the steady state for 0.5 Vol. % for 25 LPH flow rate

Time (minutes)	Inlet fluid (°C)	Surface temperature Outer side (°C)						Outlet Fluid (°C)	Pressure drop (mm)
	T_1	T_2	T_3	T_4	T_5	T_6	T_7	T_8	h
15	32.6	33.9	35.5	36.2	37.4	38.7	39.3	37.5	4.8
30	32.3	34.5	37.6	42.7	44.5	49.6	51.1	43.1	4.8
45	32.6	35.8	38.7	43.5	50.9	54.9	56.7	46.7	4.8
60	32.9	36.1	40.1	45.1	51.1	55.3	69.9	48.2	4.8
75	33.1	38.3	41.5	46.2	52.2	56.2	62.5	49.3	4.8
90	33.2	37.9	42.7	47.3	52.8	57.1	63.9	51.8	4.8
105	33.2	37.9	42.7	47.3	52.8	57.1	63.9	51.8	4.8

Table: showing reading of the steady state for 0.5 Vol. % for 30 LPH flow rate

Time (minutes)	Inlet fluid (°C)	Surface temperature Outer side (°C)						Outlet Fluid (°C)	Pressure drop (mm)
	T_1	T_2	T_3	T_4	T_5	T_6	T_7	T_8	h
15	32.1	33.1	35.4	36.2	37.6	38.4	39.7	37.6	5.5
30	32.2	34.3	36.6	38.7	43.5	44.7	49.1	43.1	5.5
45	32.3	35.6	38.7	39.5	46.9	48.9	56.7	46.7	5.5
60	32.4	36.1	39.1	41.1	48.1	50.3	58.9	47.2	5.5
75	32.6	38.2	40.5	44.2	49.2	53.8	60.5	48.7	5.5
90	32.8	37.1	41.3	45.6	50.9	54.3	62.3	50.9	5.5
105	32.8	37.1	41.3	45.6	50.9	54.3	62.3	50.9	5.5